MATHEMATICAL ENGINEERING
TECHNICAL REPORTS

Optimal Design of Periodic Frame Structures with Negative Thermal Expansion via Mixed Integer Programming

Masayuki HIROTA and Yoshihiro KANNO

METR 2014–02 January 2014

DEPARTMENT OF MATHEMATICAL INFORMATICS
GRADUATE SCHOOL OF INFORMATION SCIENCE AND TECHNOLOGY
THE UNIVERSITY OF TOKYO
BUNKYO-KU, TOKYO 113-8656, JAPAN

WWW page: http://www.keisu.t.u-tokyo.ac.jp/research/techrep/index.html

Optimal Design of Periodic Frame Structures with Negative Thermal Expansion via Mixed Integer Programming

Masayuki Hirota and Yoshihiro Kanno †

Department of Mathematical Informatics,
University of Tokyo, Tokyo 113-8656, Japan

Abstract

When structures and microstructures consisting of two or more materials with positive thermal expansion have specific configurations, they are able to have negative thermal expansion coefficients, i.e., they contract when heated. This paper proposes a topology optimization methodology of frame structures for designing a planar periodic structure that exhibits negative thermal expansion property. Provided that beam section of each existing member is chosen from a set of finitely many predetermined candidates, we show that this topology optimization problem with multiple material phases can be formulated as a mixed-integer linear programming problem. A global optimal solution can hence be found with a readily available software package. Since the proposed method treats frame structures and addresses local stress constraints, the optimal solution contains neither thin members nor hinge-like regions. To avoid too complicated structural designs realized as assemblage of many small pieces, this paper develops the constraints that separate distributions of two different materials. Numerical experiments are performed to show that structures with negative or near zero thermal expansion can be obtained by the proposed method.

Keywords

Negative thermal expansion; thermal contraction; topology optimization; mixed integer optimization; design-dependent loads.

1 Introduction

There exist many engineering structures that undergo large thermal stresses due to large temperature changes. For instance, the surface of a hypersonic cruise vehicle may be above 1000 °C due to viscous heating, which makes crucial thermal expansion mismatch between the vehicle interior; see Steeves and Evans [61] and the references therein. Ducted exhaust systems of engines of low-observable aircrafts are also subjected to very large thermal stresses [11]. Other examples include aerospace structures subjected to non-uniform heating, such as satellite telescope structures [29] and lattice structures for supporting satellite antennae and photovoltaic arrays [45]. These structures undergo large temperature differences between sunny and shady sides. In such a situation, materials and/or structures with (nearly) zero thermal expansion properties are attractive.

†Corresponding author. Address: Department of Mathematical Informatics, Graduate School of Information Science and Technology, University of Tokyo, Tokyo 113-8656, Japan. E-mail: kanno@mist.i.u-tokyo.ac.jp. Phone: +81-3-5841-6906. Fax: +81-3-5841-6886.

The majority of materials have positive thermal expansion coefficients. Materials with negative thermal expansion coefficients will contract when they are heated. Some materials, e.g., zirconium tungstate family [15, 42, 50, 59] and a number of zeolites [37], have negative thermal expansion coefficients. Such materials might be used, together with conventional materials, to make composites have any desired thermal expansion properties. As another application, Sleight [59] mentioned that sensitive temperature sensors can be made by combining thin films of materials with large positive and large negative thermal expansion properties. Thermal contraction property also has an application to thermal fasteners, which can be inserted into a hole at high temperature and fits tightly into the hole when it cools down [57]. See [4, 14, 40, 44, 59] for extensive surveys on negative thermal expansion solids.

Using two constituents with different positive thermal expansion coefficients, one can design three-phase materials, i.e., composites of two constituents combined with empty spaces, so as to have overall negative thermal expansion coefficients [19, 35, 58]. Sigmund and Torquato [57, 58] actually found such designs of three-phase composites by solving three-phase topology optimization problems. Chen *et al.* [9] also showed that microstructures with unusual thermoelastic properties can be found by using topology optimization. Subsequently, various types of negative thermal expansion composites, consisting of positive thermal expansion materials, have been proposed; e.g., sandwich composite structures [23], composites with needle-like inclusions [20], and the ones with disc and cylindrical shaped inclusions [21]. Also, periodic lattice structures consisting of two positive thermal expansion materials have been attracted much attention. Lakes [35] and Jefferson *et al.* [30] presented bi-material lattices that can exhibit negative thermal expansion properties. Grima *et al.* [22] showed that a simple periodic truss structure consisting of three different materials can have wide range of, positive and negative, thermal expansion properties. Lim [38, 39] presented two-material periodic hinged structures that can exhibit negative thermal expansion. Steeves *et al.* [60] designed two-material periodic lattice structures that has near-zero thermal expansion together with high stiffness. Miller *et al.* [43] performed tailoring thermal expansion property of a three-bar truss, one member of which consists of a material different from the other two members. This unit triangle truss can be tessellated into more complex structures.

Many studies have been done concerning structural optimization under thermal loads. Thermal stress is a typical design-dependent load. As early works, Rodrigues and Fernandes [53] developed homogenization method for topology optimization of thermoelastic structures and Jog [31] treated material and geometrical nonlinearity. Topology optimization has been used to design thermally actuated compliant mechanisms [36, 55]. Recent studies on optimization of thermoelastic structures include Deaton and Grandhi [11], Deng *et al.* [12], Gao and Zhang [17], Pedersen and Pedersen [46, 47], Wang *et al.* [70], and Xia and Wang [71]. Among them, Pedersen and Pedersen [46] discussed that, for maximizing strength of thermoelastic structures, minimization of compliance is questionable and attempted to find a design with uniform energy density. Deng *et al.* [12] optimized an overall thermoelastic structure and its material microstructure simultaneously.

There might exist some links between negative thermal expansion and negative Poisson's ratio properties; see, e.g., [5, 20, 38, 43]. Recently Kureta and Kanno [33] proposed a topology optimization method of frame structures to design a periodic planar structure that exhibits negative Poisson's ratio property. In this method, the optimization problem is recast as a *mixed-integer lin-*

ear programming (MILP) problem and is solved globally. The optimal solution has neither hinges nor thin members and local stress constraints were fully addressed in optimization. The computed optimal solution was actually fabricated by applying a photo-etching technique to a steel plate. It was confirmed that the fabricated model actually exhibits negative Poisson's ratio property. In continuation of this previous work, the present paper develops an MILP approach to designing a planar periodic frame structure that exhibits negative thermal expansion property. We suppose that a periodic frame structure is constructed by connecting a unique base cell, i.e., the smallest unit, and that each member of the frame structure consists of either one of given two different positive thermal expansion materials or void. Based upon the conventional ground structure method, topology of the base cell is optimized to minimize its thermal expansion coefficient. Material selection for each member, from among the two materials and void, is handled directly by using discrete design variables. Local stress constraints are imposed on existing members. Small deformation is assumed throughout the paper and issues of material and geometrical nonlinearity are nod addressed. A global optimal solution is then found with an existing algorithm for MILP; several software packages, e.g., CPLEX [28], are available for this purpose. The MILP formulation presented in this paper is viewed as a natural extension of the one for frame optimization proposed in [33]. Similar MILP formulations for structural optimization were developed for continua with binary design variables [64, 66], trusses with discrete member cross-sectional areas [51], and tensegrity structures [32].

Continuum topology optimization for achieving negative thermal expansion property sometimes results in very complicated structural designs. Also, the obtained structures often have hinge-like regions. Such designs may in practice require manual post-processing before actual fabrication process. For instance, Qi and Halloran [49] used a microfabrication by an oxide co-extrusion technique to fabricate the optimal design obtained by Chen *et al.* [9] and mentioned that "an engineering interpretation of the theoretical design" was necessary for strengthening some weak parts and smoothing material distribution. It is actually often that optimal solutions, obtained by continuum topology optimization, have hinge-like regions, because hinges help thermal contraction deformation to attain extremum. Thickness of hinges of an optimal solution should be adjusted carefully before fabrication process, because a structure with thin hinges can sustain only small forces while by thickening hinges the structure may lose basic feature from which negative thermal expansion accrues. One possible remedy for this issue might be to use a special technique to avoid hinge-like regions; hinge-free optimization is a current active research topic in continuum topology optimization [48, 56, 72, 74]. Alternatively, this paper proposes to use topology optimization of frame structures. In our approach, local stress constraints are fully addressed in the optimization process. Also, the section of each member is chosen from predetermined candidates. Consequently, the optimal solution has neither hinges nor thin members and, hence, may be able to be fabricated without manual post-processing, like the one with negative Poisson's ratio obtained in the previous work [33]. It should be mentioned that topology optimization of continuum structures with local stress constraints have been a challenging problem and various approaches have still been examined; see, e.g., [3, 6, 10, 13, 24, 26] and the references therein. Most of existing studies on local stress constraints consider single-material phase topology optimization problems.

The paper is organized as follows. Section 2 presents a concept of design problem of a periodic frame structure exhibiting negative thermal expansion behavior. Section 3 recasts this design prob-

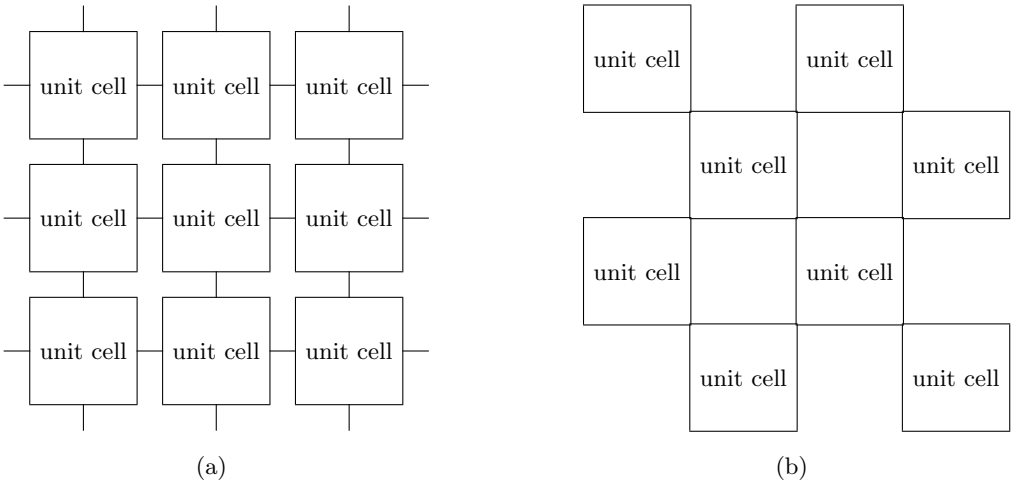

Figure 1: Two types of repeated frame structures obtained by connecting unit base cells. (a) Connection pattern (A); and (b) connection pattern (B).

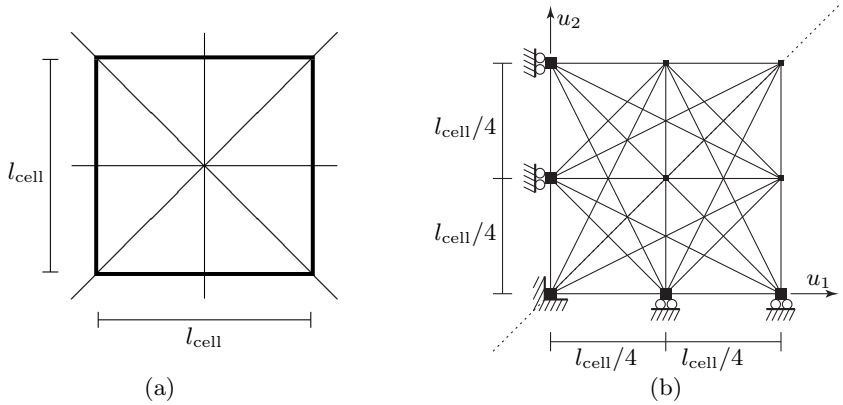

Figure 2: Problem setting. (a) A unit base cell and symmetry axes; and (b) an example of ground structure.

lem as an MILP problem. Section 4 develops an alternative formulation to obtain a base cell such that the distributions of the two different materials are clearly separated. Section 5 demonstrates numerical experiments. We conclude in section 6.

2 Design problem of structures with negative thermal expansion

Section 2.1 presents a concept of design problem of a planar periodic frame structure with negative thermal expansion coefficient property. Section 2.2 formulates an optimization problem of a base cell frame structure, where structural topology and material distribution are simultaneously optimized.

2.1 Periodic frame structure

We consider a planar frame structure realized by arranging a basic frame unit repeatedly. The properties of this frame structure are described as follows.

(i) The structure has periodicity such that a unique base cell, i.e., the smallest square unit,

is connected repeatedly in a regular way.

(ii) As for connection pattern of base cells, we consider two cases in Figure 1. In the case of pattern (A), we add four short beams to a base cell as shown in Figure 1(a), in order to connect the cell to adjacent ones. In the case of pattern (B) in Figure 1(b), the nodes at the four corners of the base cell serve as interfaces for connection.

(iii) Thermal deformation of the base cell is supposed to have square symmetry.

(iv) The whole periodic structure consisting of the base cells will contract when temperature is elevated from the ordinary value.

The design domain of our design problem is the base cell shown in Figure 2(a), due to the periodicity property in (i). To realize the symmetry property in (iii), we suppose that configuration of the unit cell is symmetric with respect to reflection across the thin lines in Figure 2(a). Figure 2(b) shows an example of ground structure, which corresponds to a quarter of the base cell in Figure 2(a). The dashed line in Figure 2(b) is an axis of symmetry of the structural design. Also, from property (iii), deformation of the whole periodic structure depends solely upon the displacements of the four nodes described in property (ii). We call these four nodes *interface nodes*. Property (iv) defines the negative thermal expansion property considered in this paper. This property can be related to the displacement of the interface node as follows. Suppose that base cells are connected according to pattern (A) in Figure 1(a). Let u_1 and u_2 denote the displacements of two interface nodes of the unit cell, as shown in Figure 2(b), when temperature increases by the specified degrees, ΔT (> 0). The side length of a unit cell is l_{cell}. From property (iii), thermoelastic deformation is symmetric, and hence $u_1 = u_2$. Hence, the side length of the cell becomes $l_{\text{cell}} + 2u_1$ due to temperature elevation ΔT. The volumetric coefficient of thermal expansion, which is given by the ratio of the area occupied by the deformed cell to the undeformed area, is written as

$$\frac{(l_{\text{cell}} + 2u_1)^2}{{l_{\text{cell}}}^2} \simeq 1 + \frac{4u_1}{l_{\text{cell}}}.$$

Therefore, the structure shows thermal contraction if the interface nodes of the base cell move inward from their positions at the ordinary temperature. This motivates us to minimize u_1 ($= u_2$) at the equilibrium state under temperature elevation ΔT. Similarly, for connection pattern (B), we can also consider a minimization problem of a displacement of a corner node of the base cell.

In designing a base cell, we explore the structure with a minimum thermal expansion coefficient by making use of some different materials with positive thermal expansion coefficients. More precisely, we determine the material that constitutes each member of the ground structure. Members will be removed if the null material is assigned. Thus we simultaneously optimize topology and material distribution of the base cell. In the course of optimization we shall make use of the following assumptions.

- Small deformations and linear elasticity are assumed.
- The base cell is supposed to consist of two different materials with positive thermal exposition coefficients.[1] Each member is thereby to be assigned either material 1, material 2, or void. Material parameters of these two materials are specified a priori.

[1] Extension of the proposed formulation to a case with more than two materials is straightforward; see Remark 3.2.

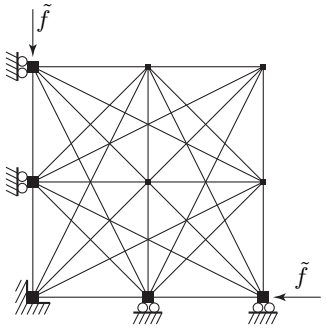

Figure 3: The fictitious forces for the compliance constraint in the case of connection pattern (A).

- At nodes of the frame structure, members constituted different materials are assumed to be bonded perfectly.
- Temperature is assumed to distribute uniformly in the frame structure.
- In the thermal deformation of each beam element, the axial extension is dominant and expansions in the other directions are assumed to be negligible.

Thus the problem dealt with in this paper is viewed as a three-phase (i.e., two materials and void) material distribution optimization on a given ground structure. For continuum structures, three-phase topology optimization has been studied extensively; see, e.g., [8, 9, 58].

As observed in [58], it is often that structures with negative thermal expansion coefficients have low global stiffness. An example is, as discussed in [60], a bi-material lattice due to Lakes [35]. For practical applications, we therefore introduce the constraint on the global stiffness in the course of optimization. Specifically, we suppose that fictitious external forces are applied to the interface nodes at the ordinary temperature as shown in Figure 3 and impose the upper bound constraint for the compliance, together with the local stress constraints. Pedersen and Pedersen [46] pointed out that, for thermoelastic structures, minimization of compliance does not necessarily result in a design with maximum strength. In this paper we consider local stress constraints, both at the elevated and ordinary temperatures, for securing structural strength directly.

Descriptive summary of the optimization problem considered in this paper is given as follows.

- Topology optimization problem of a planar frame structure is solved to obtain a base cell. Selection of materials, including the null material, for each beam element is considered a design variable. The material parameters of the constituent materials are specified.
- The displacement of the interface node induced by the temperature increase is minimized.
- The section of each existing beam element is specified.[2]
- Compliance constraint is considered for the external forces applied to the interface nodes.
- Stress constraints of existing beam elements are fully addressed.

[2]Extension of the proposed formulation to a case with more than one available beam sections is straightforward; see Remark 2.1.

- Existence of mutually intersecting beam elements is not allowed.

In the optimization process, selection of constituent materials is handled by using some discrete design variables. We solve the optimization problem within the framework of mixed integer programming. Usually, in topology optimization of continua, material selection is handled with an interpolation and penalization scheme of material constants. As an extension of the standard SIMP (solid isotropic material with penalization) scheme for interpolation, Sigmund and Torquato [58] and Gibiansky and Sigmund [18] presented a three-phase (i.e., two materials and void) topology optimization method. In this method, two variables are used for each finite element, where one of them determines whether the element is void or not and the other interpolates the material constants of the two constituent materials. This interpolation scheme was further extended to optimization with arbitrary many materials by Stegmann and Lund [63]. An extension of the RAMP (rational approximation of material properties) scheme to multiple material phases is due to Hvejsel and Lund [27]. Bruyneel [7] proposed to use shape functions of finite element method to represent the weights in material interpolation. Multi-material topology optimization was also treated within the frameworks of level-set methods [69] and phase field methods [73]. For instance, in the multi-phase level set method due to Wang and Wang [69], one material domain is represented as a union of level sets of some different implicit functions. In contrast to the literature cited above, the approach presented in this paper does not resort to any interpolation or penalization techniques but directly solves an optimization problem with discrete design variables. Since the optimization problem is recast as an MILP problem, a global optimal solution can be found by using, e.g., a branch-and-cut method. This guaranteed global optimality might be considered a major advantage of the proposed method to the existing methods using interpolation and penalization. Instead, a potential disadvantage of the proposed method is that computational cost to solve the optimization problem might increase drastically as the number of discrete design variables increases. This is because algorithms for MILP are essentially based on enumeration of solutions.

Remark 2.1. Suppose that section of each member of the base cell is chosen from a set of some (i.e., finitely many) predetermined candidates. Then the design optimization problem can still be formulated as an MILP problem. For simple presentation, however, this paper discusses only the case where single candidate is given for each member. Extension to the case with more than one candidate sections can be done in a manner similar to [33]. ■

2.2 Definition of optimization problem

This section presents an explicit form of optimization problem for the design problem sketched in section 2.1.

Consider a planar frame structure that serves as a ground structure. Figure 2(b) shows an example. The ground structure consists of many candidate members. Each member is modeled as a Timoshenko beam element. Locations of nodes are specified. Let $\mathcal{E}$ and $\mathcal{V}$ denote the set of members and the set of nodes, respectively. For example, the ground structure in Figure 2(b) consists of $|\mathcal{E}| = 28$ members and $|\mathcal{V}| = 9$ nodes.

Suppose that the material of each member is chosen among "material 1" and "material 2." Let $\mathcal{M}_1$ and $\mathcal{M}_2$ denote the sets of members constituted by material 1 and material 2, respectively. We

use $\mathcal{N}$ to denote the set of members removed as a result of optimization. Then the design problem is regarded as a problem finding a partition

$$\mathcal{E} = \mathcal{M}_1 \cup \mathcal{M}_2 \cup \mathcal{N} \tag{1}$$

of $\mathcal{E}$, where $\mathcal{M}_1$, $\mathcal{M}_2$, and $\mathcal{N}$ are disjoint sets. Material parameters of the constituent materials, listed in Table 1, are specified.

As discussed in section 2.1, we attempt to minimize the target displacement induced by the thermal increase to find the structure with the minimum thermal expansion behavior. Consider the equilibrium state of the frame structure when increase in temperature of ΔT degrees is given. Let $\boldsymbol{u} \in \mathbb{R}^d$ denote the vector of nodal displacements, where d is the number of degree of freedom of displacements. It should be clear that $\boldsymbol{u} = \boldsymbol{0}$ when no external load is applied at the ordinary temperature. For member $e \in \mathcal{E}$, let E_e, G_e, and α_e denote the Young modulus, shear modulus, and thermal expansion coefficient, respectively. For notational convenience, we use vectors $\boldsymbol{E} = (E_e \mid e \in \mathcal{E})$, $\boldsymbol{G} = (G_e \mid e \in \mathcal{E})$, and $\boldsymbol{\alpha} = (\alpha_e \mid e \in \mathcal{E})$. We use $K(\boldsymbol{E}, \boldsymbol{G}) \in \mathbb{R}^{d \times d}$ to denote the stiffness matrix. The equation of thermoelastic equilibrium may be written as

$$K(\boldsymbol{E}, \boldsymbol{G})\boldsymbol{u} - \boldsymbol{t}(\boldsymbol{\alpha}, \Delta T) = \boldsymbol{0}, \tag{2}$$

where $\boldsymbol{t}(\boldsymbol{\alpha}, \Delta T) \in \mathbb{R}^d$ is the vector of thermal forces. Explicit expression of (2) will be presented in section 3.1. Thus we attempt to minimize u_1 in Figure 2(b) under constraint (2). Here, it should be clear that E_e, G_e, and α_e depend on selection of the material that constitutes member e. Precisely, we have that $E_e = \bar{E}_1$ if $e \in \mathcal{M}_1$, $E_e = \bar{E}_2$ if $e \in \mathcal{M}_2$, and $E_e = 0$ if $e \in \mathcal{N}$. In the same manner, G_e and α_e are treated as discrete design variables.

The sections of existing members ($e \notin \mathcal{N}$) are specified a priori. Let $\bar{A}$, $\bar{I}$, and $\bar{Z}$ denote the specified cross-sectional area, moment of inertia, and elastic section modulus, respectively. We use κ to denote the shear correction factor in the Timoshenko beam theory. These parameters are treated as constants in the optimization problem.

We next consider the compliance constraint. Without taking into account the global stiffness of the structure, the topology optimization problem that minimizes the target displacement has meaningless optimal solutions. As an extreme example, if all the members of the ground structure vanish, then the target node can move freely. Such a solution is optimal and, hence, the optimal value is not bounded below. To make the optimization problem meaningful and, more practically, to find solutions with enough global stiffness, we use the upper bound constraint of the compliance. Suppose that, at the ordinary temperature, external forces are applied to the interface nodes as

Table 1: The material parameters of the constituent materials.

Material parameter	$\mathcal{M}_1$	$\mathcal{M}_2$	$\mathcal{N}$
Young's modulus	$\bar{E}_1$	$\bar{E}_2$	0
Shear modulus	$\bar{G}_1$	$\bar{G}_2$	0
Thermal expansion coefficient	$\bar{\alpha}_1$	$\bar{\alpha}_2$	0
Yield stress	$\bar{\sigma}_1^{\mathrm{y}}$	$\bar{\sigma}_2^{\mathrm{y}}$	0

shown in Figure 3. We use $\tilde{\boldsymbol{f}} \in \mathbb{R}^d$ to denote this external load. The displacement vector, $\tilde{\boldsymbol{u}} \in \mathbb{R}^d$, at the equilibrium state in the presence of $\tilde{\boldsymbol{f}}$ is obtained from

$$K(\boldsymbol{E}, \boldsymbol{G})\tilde{\boldsymbol{u}} = \tilde{\boldsymbol{f}}. \tag{3}$$

It should be clear that $\tilde{\boldsymbol{u}}$ is different from the solution, $\boldsymbol{u}$, of (2); the latter is the displacement induced by the thermal change when no external force is applied. The compliance constraint is then written as

$$\tilde{\boldsymbol{f}}^\top \tilde{\boldsymbol{u}} \leq c^{\mathrm{u}}, \tag{4}$$

where $c^{\mathrm{u}} > 0$ is the specified upper bound.

Stress constraints are formulated as follows. Consider member $e = (i, j) \in \mathcal{E}$, which connects node i and node j ($i,\ j \in \mathcal{V}$). Let $m_e^{(i)}$ and $m_e^{(j)}$ denote the two end moments. We use q_e to denote the axial force. Since members are subjected to nodal loads only, the stress constraints are considered only at the two ends of member e. Based upon a simple piecewise-linear model of yield condition, stress constraint can be written as

$$\frac{|q_e|}{\bar{A}} + \frac{\max\{|m_e^{(i)}|, |m_e^{(j)}|\}}{\bar{Z}} \leq \sigma_e^{\mathrm{u}}. \tag{5}$$

The upper bound for stress, σ_e^{u}, depends on the material constituting member e as

$$\sigma_e^{\mathrm{u}} = \begin{cases} \bar{\sigma}_1^{\mathrm{u}} & \text{if } e \in \mathcal{M}_1, \\ \bar{\sigma}_2^{\mathrm{u}} & \text{if } e \in \mathcal{M}_2, \\ 0 & \text{if } e \in \mathcal{N}, \end{cases} \tag{6}$$

where $\bar{\sigma}_1^{\mathrm{u}}$ and $\bar{\sigma}_2^{\mathrm{u}}$ are positive constants.[3] For notational convenience, define $\varphi : \mathbb{R}^3 \to \mathbb{R}$ by

$$\begin{aligned} \varphi(q_e, m_e^{(i)}, m_e^{(j)}) &= \frac{|q_e|}{\bar{A}} + \frac{\max\{|m_e^{(i)}|, |m_e^{(j)}|\}}{\bar{Z}} \\ &= \frac{|q_e|}{\bar{A}} + \frac{1}{2}\frac{|m_e^{(i)} + m_e^{(j)}|}{\bar{Z}} + \frac{1}{2}\frac{|m_e^{(i)} - m_e^{(j)}|}{\bar{Z}}. \end{aligned} \tag{7}$$

Then (5) is written as

$$\varphi(q_e, m_e^{(i)}, m_e^{(j)}) \leq \sigma_e^{\mathrm{u}}. \tag{8}$$

Presence of mutually intersecting members should be avoided. Let $\mathcal{E}_{\mathrm{cross}}$ denote the set of pairs of members that mutually intersect in the ground structure. Namely, we write $(e, e') \in \mathcal{E}_{\mathrm{cross}}$ if member e and member e' intersect. Then at least one of these two members should belong to $\mathcal{N}$. This condition is further equivalent to

$$\{e, e'\} \not\subseteq \mathcal{M}_1 \cup \mathcal{M}_2, \quad \forall (e, e') \in \mathcal{E}_{\mathrm{cross}}.$$

[3] For example, we may determine $\bar{\sigma}_1^{\mathrm{u}}$ and $\bar{\sigma}_2^{\mathrm{u}}$ from the yield stresses of the materials and a safety factor; see Remark 2.2.

By summing up the results in this section, the optimization problem to be solved is formulated as follows.

$$
\begin{aligned}
\min \quad & u_1 && && \text{(9a)}\\
\text{s.t.} \quad & K(\boldsymbol{E},\boldsymbol{G})\boldsymbol{u} - \boldsymbol{t}(\boldsymbol{\alpha},\Delta T) = \boldsymbol{0}, && && \text{(9b)}\\
& \varphi(q_e(\boldsymbol{u}), m_e^{(i)}(\boldsymbol{u}), m_e^{(j)}(\boldsymbol{u})) \le \sigma_e^{\mathrm{u}}, && \forall e=(i,j)\in\mathcal{E}, && \text{(9c)}\\
& K(\boldsymbol{E},\boldsymbol{G})\tilde{\boldsymbol{u}} = \tilde{\boldsymbol{f}}, && && \text{(9d)}\\
& \tilde{\boldsymbol{f}}^{\top}\tilde{\boldsymbol{u}} \le c^{\mathrm{u}}, && && \text{(9e)}\\
& \varphi(q_e(\tilde{\boldsymbol{u}}), m_e^{(i)}(\tilde{\boldsymbol{u}}), m_e^{(j)}(\tilde{\boldsymbol{u}})) \le \sigma_e^{\mathrm{u}}, && \forall e=(i,j)\in\mathcal{E}, && \text{(9f)}\\
& \{e,e'\} \not\subseteq \mathcal{M}_1\cup\mathcal{M}_2, && \forall (e,e')\in\mathcal{E}_{\mathrm{cross}}, && \text{(9g)}\\
& (\alpha_e, E_e, G_e, \sigma_e^{\mathrm{u}}) = \begin{cases} (\bar{\alpha}_1,\bar{E}_1,\bar{G}_1,\bar{\sigma}_1^{\mathrm{u}}) & \text{if } e\in\mathcal{M}_1,\\ (\bar{\alpha}_2,\bar{E}_2,\bar{G}_2,\bar{\sigma}_2^{\mathrm{u}}) & \text{if } e\in\mathcal{M}_2,\\ (0,0,0,0) & \text{if } e\in\mathcal{N}, \end{cases} && \forall e\in\mathcal{E}. && \text{(9h)}
\end{aligned}
$$

In this problem, we select the constituent material of each member according to (9h), where $\{\mathcal{M}_1,\mathcal{M}_2,\mathcal{N}\}$ is a partition of $\mathcal{E}$. Constraints (9b) and (9c) are concerned with the equilibrium state at the high temperature, and thence the minimal thermal expansion property is achieved by minimizing u_1. Constraints (9d), (9e), and (9f) are concerned with the equilibrium state at the ordinary temperature, where the fictitious external load, $\tilde{\boldsymbol{f}}$, is applied. Constraints on the compliance and member stresses are considered. Presence of mutually intersecting members is forbidden by (9g).

Remark 2.2. Stress constraint (5) has been derived as follows. Let $\bar{\sigma}_p^{\mathrm{y}}$ denote the yield stress of material p ($p=1,2$), which is a given constant. The upper bound stress, $\bar{\sigma}_p^{\mathrm{u}}$, may be determined as

$$\bar{\sigma}_p^{\mathrm{u}} = \bar{\sigma}_p^{\mathrm{y}}/\gamma,$$

where $\gamma\ge 1$ is a specified safety factor. Then the upper bound stress of member $e=(i,j)$ is defined by (6). The upper bounds for absolute values of the axial force and the end moment, denoted q_e^{u} and m_e^{u}, are given by

$$q_e^{\mathrm{u}} = \sigma_e^{\mathrm{u}}\bar{A}, \quad m_e^{\mathrm{u}} = \sigma_e^{\mathrm{u}}\bar{Z}. \tag{10}$$

The stress constraints are written at both ends of the member as

$$\frac{|q_e|}{q_e^{\mathrm{u}}} + \frac{|m_e^{(i)}|}{m_e^{\mathrm{u}}} \le 1, \quad \frac{|q_e|}{q_e^{\mathrm{u}}} + \frac{|m_e^{(j)}|}{m_e^{\mathrm{u}}} \le 1. \tag{11}$$

By substituting (10) into (11) and putting together the two inequalities, we obtain (5). ■

Remark 2.3. Generally speaking, in topology optimization the stress constraint should be imposed only on existing members. In other words, if member e vanishes in the course of optimization, i.e., if $e\in\mathcal{N}$, then the stress constraint on member e should be removed from the optimization problem [2, 10, 54]. It should be clear that in this section the stress constraints, i.e., (9c) and (9f), have been formulated in terms of the axial force and the two end moments. In the course optimization, all the members have a specified common section, i.e., $\bar{A}$, $\bar{I}$, and $\bar{Z}$ are considered

constants, while the material parameters for $e \in \mathcal{N}$ are $\alpha_e = E_e = G_e = 0$. Therefore, if $e = (i, j) \in \mathcal{N}$, then we obtain

$$q_e(\boldsymbol{u}) = m_e^{(i)}(\boldsymbol{u}) = m_e^{(j)}(\boldsymbol{u}) = 0.$$

This implies that adding the condition

$$\varphi(q_e, m_e^{(i)}, m_e^{(j)}) \leq 0, \quad \forall e \in \mathcal{N} \tag{12}$$

to the optimization problem as the constraints does not change the feasible set. Condition (12) has been actually incorporated in (9c) and (9f). ■

Remark 2.4. As explained in section 2.1, the configuration of the unit cell is set to be symmetric with respect to the dashed line in Figure 2(b). This constraint is formally written as follows. Let $\mathcal{E}_{\mathrm{sym}}$ denote the set of pairs of members that are located at symmetric positions. Namely, we write $(e, e') \in \mathcal{E}_{\mathrm{sym}}$ if member e is swapped with member e' by reflection depicted in Figure 2(b). Then these two members should have the same material selection, i.e., each $(e, e') \in \mathcal{E}_{\mathrm{sym}}$ should satisfy

$$e \in \mathcal{M}_1 \quad \Leftrightarrow \quad e' \in \mathcal{M}_1, \tag{13a}$$
$$e \in \mathcal{M}_2 \quad \Leftrightarrow \quad e' \in \mathcal{M}_2, \tag{13b}$$
$$e \in \mathcal{N} \quad \Leftrightarrow \quad e' \in \mathcal{N}. \tag{13c}$$

In practice, this condition is added to problem (9) as a constraint. ■

3 Mixed-integer linear programming approach

In this section we present an MILP approach to the design optimization problem for finding frame structures with negative thermal expansion properties. As mentioned in section 2.2, in this design problem each member belongs either $\mathcal{M}_1$, $\mathcal{M}_2$, or $\mathcal{N}$. We express this choice by making use of two 0–1 design variables. Section 3.1 presents explicit forms of the constraints of problem (9). Section 3.2 reformulates problem (9) as an MILP problem.

3.1 Thermoelastic equilibrium equations with material selection

In this section we write the constraints of problem (9) explicitly as preparation for the MILP formulation presented in section 3.2. Particular attention is focused on the thermoelastic equilibrium equation, (9b), in conjunction with the material selection constraint, (9h). A key is the decomposition of the stiffness matrix of a frame structure, which was used also in [33]. Two differences from the previous formulation in [33] are that we now consider thermal effect and material selection.

According to section 3.2 of [33], the equilibrium equation,

$$K(\boldsymbol{E}, \boldsymbol{G})\boldsymbol{u} = \boldsymbol{f}, \tag{14}$$

is decomposed into the force-balance equation written as

$$\sum_{e \in \mathcal{E}} \sum_{t=1}^{3} s_{et} \boldsymbol{b}_{et} = \boldsymbol{f} \tag{15}$$

and the relations between the generalized stresses and the displacement vector written as

$$s_{et} = k_{et}\boldsymbol{b}_{et}^{\top}\boldsymbol{u}. \quad t = 1, 2, 3;\ \forall e \in \mathcal{E}. \tag{16}$$

Here, $\boldsymbol{b}_{e1}$, $\boldsymbol{b}_{e2}$, $\boldsymbol{b}_{e3} \in \mathbb{R}^d$ ($\forall e \in \mathcal{E}$) are constant vectors. Constants k_{e1}, k_{e2}, $k_{e3} \in \mathbb{R}$ ($\forall e \in \mathcal{E}$) are defined by

$$k_{e1} = \frac{E_e A_e}{l_e}, \tag{17a}$$

$$k_{e2} = \frac{1}{l_e}\Big(\frac{l_e^2}{12E_eI_e} + \frac{1}{\kappa G_e A_e}\Big)^{-1}, \tag{17b}$$

$$k_{e3} = \frac{E_e I_e}{l_e}, \tag{17c}$$

where A_e is the cross-sectional area, I_e is the moment of inertia, and l_e is the undeformed length of beam element e. In (17b), we define $k_{e2} = 0$ if $E_e = G_e = 0$ for convention. By eliminating s_{et}'s, we see that (15) and (16) revert to (14). Expression in (15) and (16) serves as basis of our MILP formulation. Details of the decomposition above appear in appendix A.

The equation of thermoelastic equilibrium, (2), can be written explicitly as follows. Let l_e denote the undeformed length of member e ($e \in \mathcal{E}$). Due to temperature change ΔT, the length of the member becomes $l_e(1 + \alpha_e \Delta T)$. Therefore, the relation between the axial force and the displacements, i.e., $t = 1$ in (16), is now given by

$$s_{e1} = k_{e1}(\boldsymbol{b}_{e1}^{\top}\boldsymbol{u}_e - l_e\alpha_e\Delta T).$$

Since we assume that thermal expansions in directions other than the axial direction are negligible, s_{e2} and s_{e3} are given by (16). Recall that, in the course of optimization, coefficients k_{e1}, k_{e2}, k_{e3}, and α_e are determined by the material selected for member e. By incorporating this selection, we see that the equation of thermoelastic equilibrium can be written explicitly as

$$\sum_{e\in\mathcal{E}}\sum_{t=1}^{3} s_{et}\boldsymbol{b}_{et} = \boldsymbol{0}, \tag{18a}$$

$$s_{e1} = \begin{cases} \bar{k}_{e11}(\boldsymbol{b}_{e1}^{\top}\boldsymbol{u} - l_e\bar{\alpha}_1\Delta T), & \text{if } e \in \mathcal{M}_1, \\ \bar{k}_{e12}(\boldsymbol{b}_{e1}^{\top}\boldsymbol{u} - l_e\bar{\alpha}_2\Delta T), & \text{if } e \in \mathcal{M}_2, \\ 0 & \text{if } e \in \mathcal{N}, \end{cases} \tag{18b}$$

$$s_{et} = \begin{cases} \bar{k}_{et1}\boldsymbol{b}_{et}^{\top}\boldsymbol{u}, & \text{if } e \in \mathcal{M}_1, \\ \bar{k}_{et2}\boldsymbol{b}_{et}^{\top}\boldsymbol{u}, & \text{if } e \in \mathcal{M}_2, \\ 0 & \text{if } e \in \mathcal{N}, \end{cases} \quad t = 2, 3, \tag{18c}$$

where constants $\bar{k}_{etp}$ ($t = 1, 2, 3;\ p = 1, 2$) are defined by

$$\bar{k}_{e1p} = \frac{\bar{E}_p\bar{A}}{l_e}, \tag{19a}$$

$$\bar{k}_{e2p} = \frac{1}{l_e}\Big(\frac{l_e^2}{12\bar{E}_p\bar{I}} + \frac{1}{\bar{G}_p\kappa\bar{A}}\Big)^{-1}, \tag{19b}$$

$$\bar{k}_{e3p} = \frac{\bar{E}_p\bar{I}}{l_e}. \tag{19c}$$

The displacement in the compliance constraint, (9e), is defined by the equilibrium equation at the ordinary temperature, (9d). By using expression in (15) and (16), (9d) can be rewritten as

$$\sum_{e\in\mathcal{E}}\sum_{t=1}^{3}\tilde{s}_{et}\boldsymbol{b}_{et}=\tilde{\boldsymbol{f}}, \tag{20a}$$

$$\tilde{s}_{et}=k_{et}\boldsymbol{b}_{et}^{\top}\tilde{\boldsymbol{u}},\quad t=1,2,3;\ e\in\mathcal{E}, \tag{20b}$$

where $k_{et}=\bar{k}_{etp}$ if $e\in\mathcal{M}_p$, otherwise $k_{et}=0$, as explicitly written in (18).

It is useful to rewrite the stress constraints, i.e., (9c) and (9f), in terms of the generalized stresses, s_{et} $(t=1,2,3)$. It follows from (7) and (45) (in appendix A) that (9c) can be rewritten as

$$\frac{|s_{e1}|}{\bar{A}}+\frac{1}{2}\frac{l_e|s_{e2}|}{\bar{Z}}+\frac{|s_{e3}|}{\bar{Z}}\le\sigma_e^{\mathrm{u}}. \tag{21}$$

Similarly, (9f) can be rewritten as

$$\frac{|\tilde{s}_{e1}|}{\bar{A}}+\frac{1}{2}\frac{l_e|\tilde{s}_{e2}|}{\bar{Z}}+\frac{|\tilde{s}_{e3}|}{\bar{Z}}\le\sigma_e^{\mathrm{u}}. \tag{22}$$

It should be clear that σ_e^{u} in (21) and (22) depends on material selection for member e; see (6).

As the upshot of this section, it is worth noting that constraints (18b), (18c), (20b), (21), and (22) involve terms depending on material selections. This reflects intrinsically combinatorial property of our design problem. In section 3.2 we shall introduce some binary variables to treat these constraints within the framework of MILP.

3.2 Reformulation to mixed-integer linear programming problem

In this section, optimization problem (9) presented in section 2.2 is reduced to an MILP problem. We make use of the formulations developed in section 3.1 for thermoelastic equilibrium equations.

As mentioned earlier, the design problem is interpreted as finding a partition of a set of members, (1), such that the objective function is minimized. A key idea to deal with this partition in our optimization problem is making use of integer variables that serve as labels of members. Specifically, we use two 0–1 variables,

$$(x_{e1},x_{e2})\in\{0,1\}^2, \tag{23}$$

to express the label of member $e\in\mathcal{E}$ as

$$(x_{e1},x_{e2})=(1,0)\quad\Leftrightarrow\quad e\in\mathcal{M}_1, \tag{24a}$$

$$(x_{e1},x_{e2})=(0,1)\quad\Leftrightarrow\quad e\in\mathcal{M}_2, \tag{24b}$$

$$(x_{e1},x_{e2})=(0,0)\quad\Leftrightarrow\quad e\in\mathcal{N}. \tag{24c}$$

These variables are subjected to the constraint

$$x_{e1}+x_{e2}\le 1. \tag{25}$$

We begin by reformulating constraint (18), i.e., the equilibrium equation at the high temperature. Since (18a) is a linear constraint, attention is focused on (18b) and (18c). By making use of x_{e1}

and x_{e2} in (24), (18b) can be rewritten as

$$|s_{e1} - \bar{k}_{e1p}(\boldsymbol{b}_{e1}^\top \boldsymbol{u} - l_e \bar{\alpha}_p \Delta T)| \le L(1 - x_{ep}), \quad p = 1, 2, \tag{26a}$$

$$|s_{e1}| \le L(x_{e1} + x_{e2}), \tag{26b}$$

where $L \gg 0$ is a sufficiently large constant. Similarly, (18c) is equivalent to

$$|s_{et} - \bar{k}_{etp}(\boldsymbol{b}_{et}^\top \boldsymbol{u})| \le L(1 - x_{ep}), \quad p = 1, 2;\ t = 2, 3, \tag{27a}$$

$$|s_{et}| \le L(x_{e1} + x_{e2}), \qquad t = 2, 3. \tag{27b}$$

We next consider the stress constraint, (21). Note that σ_e^{u} in (21) is defined by (6), i.e.,

$$\sigma_e^{\mathrm{u}} = \bar{\sigma}_1^{\mathrm{u}} x_{e1} + \bar{\sigma}_2^{\mathrm{u}} x_{e2}.$$

Hence, (21) is equivalent to

$$\frac{|s_{e1}|}{\bar{A}} + \frac{l_e |s_{e2}|}{2\bar{Z}} + \frac{|s_{e3}|}{\bar{Z}} \le \bar{\sigma}_1^{\mathrm{u}} x_{e1} + \bar{\sigma}_2^{\mathrm{u}} x_{e2}. \tag{28}$$

Constraint (22) can be rewritten by using x_{e1} and x_{e2} similarly. By imposing (28) on the optimization problem as a constraint, constraints (26b) and (27b) become redundant and, thence, are omitted.

Constraint (9g), which avoids existence of mutually intersecting members, can also be written in terms of x_{e1} and x_{e2}. Observe that $x_{e1} + x_{e2} = 1$ holds if and only if $e \in \mathcal{M}_1 \cup \mathcal{M}_2$. Therefore, (9g) is equivalent to

$$x_{e1} + x_{e2} + x_{e'1} + x_{e'2} \le 1, \quad \forall (e, e') \in \mathcal{E}_{\mathrm{cross}}. \tag{29}$$

By summing up the results above, problem (9) is reduced to the following MILP problem:

$$\min \quad u_1 \tag{30a}$$

$$\text{s.t.} \quad \sum_{e \in \mathcal{E}} \sum_{t=1}^{3} s_{et} \boldsymbol{b}_{et} = \boldsymbol{f}, \tag{30b}$$

$$|s_{e1} - \bar{k}_{e1p}(\boldsymbol{b}_{e1}^\top \boldsymbol{u} - l_e \bar{\alpha}_p \Delta T)| \le L(1 - x_{ep}), \quad p = 1, 2;\ \forall e, \tag{30c}$$

$$|s_{et} - \bar{k}_{etp} \boldsymbol{b}_{et}^\top \boldsymbol{u}| \le L(1 - x_{ep}), \quad t = 2, 3;\ p = 1, 2;\ \forall e, \tag{30d}$$

$$\frac{|s_{e1}|}{\bar{A}} + \frac{l_e |s_{e2}|}{2\bar{Z}} + \frac{|s_{e3}|}{\bar{Z}} \le \sum_{p=1}^{2} \bar{\sigma}_p^{\mathrm{u}} x_{ep}, \quad \forall e, \tag{30e}$$

$$\sum_{e \in \mathcal{E}} \sum_{t=1}^{3} \tilde{s}_{et} \boldsymbol{b}_{et} = \tilde{\boldsymbol{f}}, \tag{30f}$$

$$|\tilde{s}_{et} - \bar{k}_{etp} \boldsymbol{b}_{et}^\top \tilde{\boldsymbol{u}}| \le L(1 - x_{ep}), \quad t = 1, 2, 3;\ p = 1, 2;\ \forall e, \tag{30g}$$

$$\tilde{\boldsymbol{f}}^\top \tilde{\boldsymbol{u}} \le c^{\mathrm{u}}, \tag{30h}$$

$$\frac{|\tilde{s}_{e1}|}{\bar{A}} + \frac{l_e |\tilde{s}_{e2}|}{2\bar{Z}} + \frac{|\tilde{s}_{e3}|}{\bar{Z}} \le \sum_{p=1}^{2} \bar{\sigma}_p^{\mathrm{u}} x_{ep}, \quad \forall e, \tag{30i}$$

$$x_{e1} + x_{e2} + x_{e'1} + x_{e'2} \le 1, \quad \forall (e, e') \in \mathcal{E}_{\mathrm{cross}}, \tag{30j}$$

$$x_{e1} + x_{e2} \le 1, \quad \forall e, \tag{30k}$$

$$x_{e1}, x_{e2} \in \{0, 1\}, \quad \forall e. \tag{30l}$$

Here, continuous variables are $\boldsymbol{u} \in \mathbb{R}^d$, $\tilde{\boldsymbol{u}} \in \mathbb{R}^d$, $s_{et} \in \mathbb{R}$, and $\tilde{s}_{et} \in \mathbb{R}$ ($\forall e \in \mathcal{E};\ t = 1, 2, 3$), while 0–1 variables are x_{e1} and x_{e2} ($\forall e \in \mathcal{E}$). All the constraints other than the integrality constraints, (30l), are linear constraints. Thus, problem (30) is an MILP problem, and hence it can be solved globally with, e.g., a branch-and-cut method. Several software packages, e.g., CPLEX [28], Gurobi Optimizer [25], and SCIP [1], are available for this purpose.

Remark 3.1. In Remark 2.4, the constraint on symmetry in configuration of the base cell was formulated as (13). This constraint can also be rewritten in terms of 0–1 variables, x_{e1} and x_{e2} ($e \in \mathcal{E}$). Recall that $(e, e') \in \mathcal{E}_{\text{sym}}$ means that member e and member e' are located at symmetric positions. Then the symmetry constraint, (13), is equivalently rewritten as

$$(x_{e1}, x_{e2}) = (x_{e'1}, x_{e'2}), \quad \forall (e, e') \in \mathcal{E}_{\text{sym}}.$$

In practice, this condition is added to problem (30) as linear equality constraints. ■

Remark 3.2. The approach developed above can be extended to a case in which more than two constituent materials are available to design a structure. For instance, suppose that three materials, i.e., $\mathcal{M}_1$, $\mathcal{M}_2$, and $\mathcal{M}_3$, are available. Contrary to (24), in this case we use three 0–1 variables to express selection of material for member e as

$$\begin{aligned}
(x_{e1}, x_{e2}, x_{e3}) = (1, 0, 0) \quad &\Leftrightarrow \quad e \in \mathcal{M}_1, \\
(x_{e1}, x_{e2}, x_{e3}) = (0, 1, 0) \quad &\Leftrightarrow \quad e \in \mathcal{M}_2, \\
(x_{e1}, x_{e2}, x_{e3}) = (0, 0, 1) \quad &\Leftrightarrow \quad e \in \mathcal{M}_3, \\
(x_{e1}, x_{e2}, x_{e3}) = (0, 0, 0) \quad &\Leftrightarrow \quad e \in \mathcal{N}.
\end{aligned}$$

Constraint (25) is then replaced with

$$x_{e1} + x_{e2} + x_{e3} \leq 1.$$

The other constraints can also be rewritten by using x_{e1}, x_{e2}, and x_{e3} ($\forall e \in \mathcal{E}$) in a straightforward manner. ■

4 Separation of material distribution domains

A base cell consists of two materials. Distributions of the materials at the optimal solution can possibly become complicated. Then the base cell becomes assemblage of many small pieces, each of which consists of single material. Such complex material distributions in a base cell may cause difficulty in manufacture of the periodic structure. This motivates us in this section to develop a formulation of the design problem that can avoid mixture of material distributions. Section 4.1 introduces binary variables used for representing the material domains on a given ground structure. Section 4.2 shows that the design optimization problem with the separation constraint on material distributions can be recast as an MILP problem.

4.1 Notion of material domains

In the formulation developed in section 3, no constraint has been considered concerning distribution pattern of the two materials. It may possibly happen that, at the optimal solution, small pieces

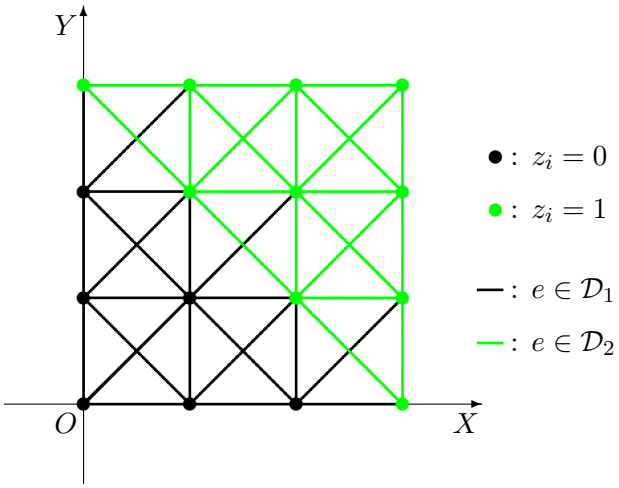

Figure 4: An example of values of z_i ($\forall i \in \mathcal{V}$) and the corresponding material domains, $\mathcal{D}_1$ and $\mathcal{D}_2$.

consisting of different materials are connected to each other and domains of the two materials are arranged in a complicated manner; see Figure 9(d) in section 5.1 for a typical example. Such complicated material distributions in a base cell can be a source of difficulty in actual fabrication process.[4] In the following, for an obtained base cell, we call the set of members consisting of single material a *material domain*. We say that two material domains are *separated* if there exists a (closed) curve that separates two domains.

Steeves *et al.* [60] used base cells with separated material domains to create planar periodic lattices exhibiting negative thermal expansion properties; subsequently, these lattices were studied further in [61, 62]. In these base cells, the material with low thermal expansion is placed outside of the material with high thermal expansion. Hence, when temperature is elevated, compression forces will act on interfaces between two different materials. Due to these compression forces, bonding between two materials will be strengthened automatically. Thus, placing the material with low thermal expansion outside of the material with high thermal expansion might have a practical advantage. In the following, we suppose $\bar{\alpha}_1 > \bar{\alpha}_2$ without loss of generality and attempt to place $\mathcal{M}_2$ outside of $\mathcal{M}_1$. Note that we do not consider explicit constraints that prohibit tension forces at interfaces between two different materials. Therefore, at the optimal solution it is not guaranteed that forces acting at those interfaces are compressive.

To separate distributions of the two materials on a ground structure, we introduce the notion of material domains as follows. Recall that $\mathcal{E}$ is the set of members of the ground structure. Consider partition $\mathcal{E} = \mathcal{D}_1 \cup \mathcal{D}_2$ of $\mathcal{E}$, where $\mathcal{D}_1$ and $\mathcal{D}_2$ are the sets of members that can be constituted by

[4]By using a modern sophisticated processing technique, we can probably fabricate periodic structures with complicated configurations. For instance, Chen *et al.* [9] used a direct metal deposition, which melts powdered metals by laser, to fabricate a periodic structure with negative thermal expansion, which was found by three-phase topology optimization. Also, Qi and Halloran [49] fabricated the structure in [9] with microfabrication by co-extrusion, which is a powder based thermoplastic processing technique. Therefore, with such a processing technique, it is probably possible to fabricate the optimal solutions obtained by using the formulation in section 3. In section 4 we attempt to find a design which can be fabricated even with a more naive technique.

material 1 and material 2, respectively. Namely, $\mathcal{M}_1$ and $\mathcal{M}_2$ should satisfy

$$\mathcal{M}_1 \subseteq \mathcal{D}_1, \quad \mathcal{M}_2 \subseteq \mathcal{D}_2.$$

For node $i \in \mathcal{V}$, let $z_i \in \{0,1\}$ be a binary variable. We represent $\mathcal{D}_1$ and $\mathcal{D}_2$ by using z_i ($\forall i \in \mathcal{V}$) as

$$z_i + z_j \leq 1 \quad \Leftrightarrow \quad e = (i,j) \in \mathcal{D}_1, \tag{31a}$$
$$z_i + z_j = 2 \quad \Leftrightarrow \quad e = (i,j) \in \mathcal{D}_2; \tag{31b}$$

see Figure 4 for an example. To place $\mathcal{M}_2$ outside of $\mathcal{M}_1$, we introduce the constraints such that nodes near the center of the base cell satisfy $z_i = 0$ and nodes exterior of the base cell satisfy $z_i = 1$. Roughly speaking, if node i is farther than node j from the origin, O, in Figure 4, then we impose the constraint

$$z_i \geq z_j; \tag{32}$$

see, for details, (39), (40), and (41) in section 4.2.

Besides z_i ($\forall i \in \mathcal{V}$), we use variable $x_e \in \{0,1\}$ which serves as an indicator of existence of member $e \in \mathcal{E}$. Namely, existence of member e is represented as

$$x_e = 1 \quad \Leftrightarrow \quad e \in \mathcal{M}_1 \cup \mathcal{M}_2, \tag{33a}$$
$$x_e = 0 \quad \Leftrightarrow \quad e \in \mathcal{N}. \tag{33b}$$

It follows from (31) and (33) that selection of the material for member e is expressed as

$$x_e = 1,\ z_i + z_j \leq 1 \quad \Leftrightarrow \quad e \in \mathcal{M}_1, \tag{34a}$$
$$x_e = 1,\ z_i + z_j = 2 \quad \Leftrightarrow \quad e \in \mathcal{M}_2, \tag{34b}$$
$$x_e = 0,\ z_i + z_j \leq 2 \quad \Leftrightarrow \quad e \in \mathcal{N}. \tag{34c}$$

In the optimization process we shall determine x_e ($\forall e \in \mathcal{E}$) and z_i ($\forall i \in \mathcal{V}$).

4.2 MILP formulation with domain separation constraint

This section demonstrates that, under the setting introduced in section 4.1, the design optimization problem can be formulated as an MILP problem. To see this, we show that the constraints in section 3.2, which have been formulated with variables $(x_{e1}, x_{e2}) \in \{0,1\}^2$ ($\forall e \in \mathcal{E}$), can now be rewritten with $x_e \in \{0,1\}$ ($\forall e \in \mathcal{E}$) and $z_i \in \{0,1\}$ ($\forall i \in \mathcal{V}$). The equilibrium equations together with the stress constraints, the compliance constraint, the constraint prohibiting intersection of members, and the constraint on symmetry in the configuration are considered. Also, we handle the constraint separating the material domains, $\mathcal{D}_1$ and $\mathcal{D}_2$. All these constraints shall be formulated as linear constraints in terms of x_e's, z_i's, and some continuous variables.

We begin by rewriting (18), i.e., the equilibrium equation at the high temperature, with binary variables x_e and z_i. Since (18a) is independent of material selection, attention is focused on (18b)

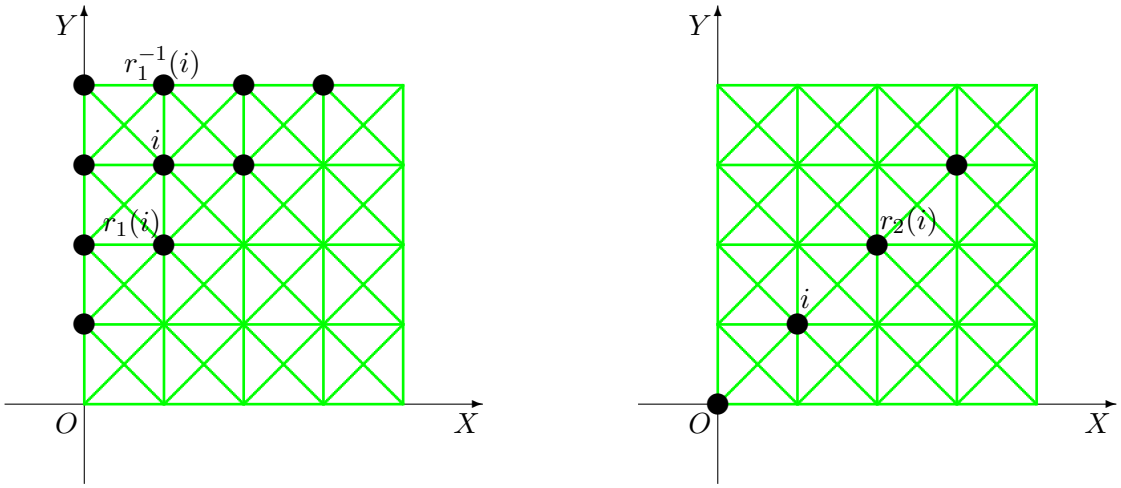

Figure 5: Notation for the domain separation constraints. (a) The set of nodes depicted by filled circles is $\mathcal{V}_{\rm upper}$; and (b) the set of nodes depicted by filled circles is $\mathcal{V}_{\rm diag}$.

and (18c). Referring to (34), we can rewrite (18b) for each $e = (i, j) \in \mathcal{E}$ as

$$|s_{e1} - \bar{k}_{e11}(\boldsymbol{b}_{e1}^\top \boldsymbol{u} - l_e \bar{\alpha}_1 \Delta T)| \le L(1 - x_e + z_i), \tag{35a}$$
$$|s_{e1} - \bar{k}_{e11}(\boldsymbol{b}_{e1}^\top \boldsymbol{u} - l_e \bar{\alpha}_1 \Delta T)| \le L(1 - x_e + z_j), \tag{35b}$$
$$|s_{e1} - \bar{k}_{e12}(\boldsymbol{b}_{e1}^\top \boldsymbol{u} - l_e \bar{\alpha}_2 \Delta T)| \le L(3 - x_e - z_i - z_j), \tag{35c}$$
$$|s_{e1}| \le L x_e, \tag{35d}$$

where $L \gg 0$ is a sufficiently large constant. In the same manner, (18c) can be reduced to linear inequality constraints by using x_e, z_i, and z_j.

We next consider the stress constraints in (21), where $\sigma_e^{\rm u}$ is defined by (6). Referring to (34), we see that (21) with (6) can be rewritten by using x_e and z_i as

$$\frac{|s_{e1}|}{\bar{A}} + \frac{l_e|s_{e2}|}{2\bar{Z}} + \frac{|s_{e3}|}{\bar{Z}} \le \bar{\sigma}_1^{\rm u}(2 - z_i - z_j) + \bar{\sigma}_2^{\rm u} z_i, \tag{36a}$$
$$\frac{|s_{e1}|}{\bar{A}} + \frac{l_e|s_{e2}|}{2\bar{Z}} + \frac{|s_{e3}|}{\bar{Z}} \le \bar{\sigma}_1^{\rm u}(2 - z_i - z_j) + \bar{\sigma}_2^{\rm u} z_j, \tag{36b}$$
$$\frac{|s_{e1}|}{\bar{A}} + \frac{l_e|s_{e2}|}{2\bar{Z}} + \frac{|s_{e3}|}{\bar{Z}} \le \bar{\sigma}_1^{\rm u}(1 + z_i + z_j) + \bar{\sigma}_2^{\rm u}(z_i + z_j). \tag{36c}$$

The equilibrium equations at the ordinary temperature are given by (20). Here, (20a) is a system of linear equality constraints. On the other hand, (20b) can be rewritten as linear inequality constraints by using x_e and z_i in the same manner as (35). Also, the stress constraints, (22), can be reformulated in the same manner as (36).

The constraint prohibiting existence of mutually intersecting member is given by (9g). By using (33), this constraint can be rewritten in terms of x_e's as

$$x_e + x_{e'} \le 1, \quad \forall (e, e') \in \mathcal{E}_{\rm cross}. \tag{37}$$

The constraint on symmetry of the base cell is formulated as follows. Unlike Remark 3.1, we now have to use variables x_e and z_i to write this constraint. Recall that $(e, e') \in \mathcal{E}_{\rm sym}$ means that

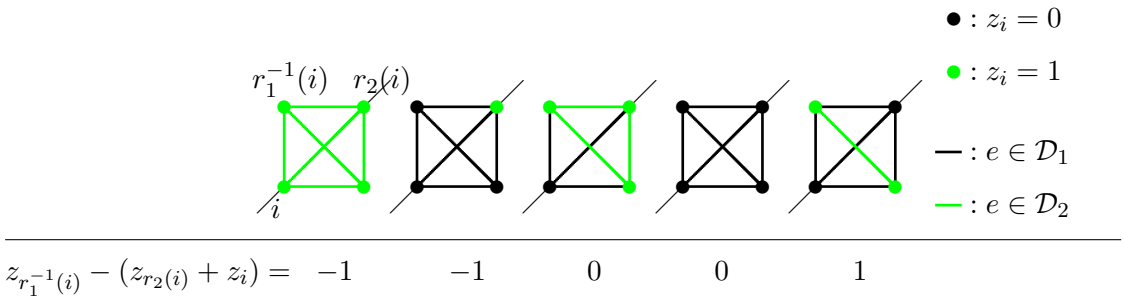

Figure 6: Enumeration of $(z_i, z_{r_1^{-1}(i)}, z_{r_2(i)})$ satisfying (39) and (40) for $i \in \mathcal{V}_{\text{diag}}$ and the corresponding material distributions. The values of $z_{r_1^{-1}(i)} - (z_{r_2(i)} + z_i)$ are listed in the bottom row.

member e and member e' are located at symmetric positions. Similarly, we write $(i, j) \in \mathcal{V}_{\text{sym}}$ if node i is swapped with node j by reflection depicted in Figure 2(b). Then the symmetry constraint is given by

$$x_e = x_{e'}, \quad \forall (e, e') \in \mathcal{E}_{\text{sym}}, \tag{38a}$$

$$z_i = z_j, \quad \forall (i, j) \in \mathcal{V}_{\text{sym}}. \tag{38b}$$

Finally we consider the constraint for separating material domains, $\mathcal{D}_1$ and $\mathcal{D}_2$. An essential idea for this constraint has been sketched in section 4.1; see (32). Explicit forms of this constraint dependent on the shape of a ground structure. In this paper we restrict ourselves to ground structures with grid shapes such as the one in Figure 4. Due to symmetry, we consider only the upper triangular portion. Firstly, let $\mathcal{V}_{\text{upper}} \subset \mathcal{V}$ denote the set of nodes that are located above the diagonal line; see Figure 5(a). For $i \in \mathcal{V}_{\text{upper}}$, the node located just below node i is called node $r_1(i)$. The X-coordinates of node i and node $r_1(i)$ are the same. Hence, node i is farther than node $r_1(i)$ from the origin, O, of the coordinate system illustrated in Figure 5. Recall that member $e = (i, j) \in \mathcal{E}$ can satisfy $(i, j) \in \mathcal{M}_2$ only if $z_i = z_j = 1$; see (31). Since we attempt to place $\mathcal{M}_2$ outside of $\mathcal{M}_1$, we require $z_{r_1}(i) = 0$ if the outside node, $i \in \mathcal{V}_{\text{upper}}$, satisfies $z_i = 0$. For this reason we consider the following constraint:

$$z_i \geq z_{r_1(i)}, \quad \forall i \in \mathcal{V}_{\text{upper}}. \tag{39}$$

Secondly, consider the nodes on the diagonal of the base cell. We denote by $\mathcal{V}_{\text{diag}} \subset \mathcal{V}$ the set of these nodes as shown in Figure 5(b). Note that we exclude the top rightmost node from $\mathcal{V}_{\text{diag}}$ for notational convenience. For $i \in \mathcal{V}_{\text{diag}}$, the diagonal node just outside of node i is called node $r_2(i)$. Node $r_2(i)$ is farther than node i from the origin, O. Hence, if $z_{r_2(i)x} = 0$, then the inside node, i, should satisfy $z_i = 0$. This motivates us to consider the following constraint:

$$z_{r_2(i)} \geq z_i, \quad \forall i \in \mathcal{V}_{\text{diag}}. \tag{40}$$

For $i \in \mathcal{V}_{\text{diag}}$, consider nodes $r_1^{-1}(i)$ and $r_2(i)$, where $r_1^{-1}(i)$ is defined by $r_1(r_1^{-1}(i)) = i$. As listed in Figure 6, there exist five cases of $(z_i, z_{r_1^{-1}(i)}, z_{r_2(i)})$ satisfying (39) and (40). Among these five patterns, only the rightmost one is not acceptable, because a member of $\mathcal{M}_2$ is surrounded by members of $\mathcal{M}_1$. It is observed from the bottom row of Figure 6 that this unacceptable pattern can be excluded by adding the following constraint:

$$z_{r_1^{-1}(i)} \leq z_{r_2(i)} + z_i, \quad \forall i \in \mathcal{V}_{\text{diag}}. \tag{41}$$

Thus all the constraints are written as linear constraints in terms of $\boldsymbol{u} \in \mathbb{R}^d$, $\tilde{\boldsymbol{u}} \in \mathbb{R}^d$, $s_{et} \in \mathbb{R}$, $\tilde{s}_{et} \in \mathbb{R}$, $x_e \in \{0,1\}$, and $s_i \in \{0,1\}$ ($\forall e \in \mathcal{E};\ \forall i \in \mathcal{V};\ t = 1,2,3$). Therefore, the optimization problem considered in this section can be recast as an MILP problem. The full description of this MILP problem appears in appendix B.

5 Numerical experiments

In this section we perform numerical experiments by solving the proposed MILP problems. Section 5.1 collects design examples of the formulation presented in section 3, i.e., problem (30), while section 5.2 collects the ones of the formulation developed in section 4. Computation was carried out on 2.66 GHz 6-Core Intel Xeon Westmere processors with 64 GB RAM. MILP problems were solved by using CPLEX ver. 12.2 [28]. As for parameters of CPLEX, the integrality tolerance and feasibility tolerance were set to $= 10^{-8}$. The other parameters of CPLEX were set to the default values.

Each existing member has a rectangular cross-section with width $\bar{w} = 1\,\mathrm{mm}$ and thickness $\bar{t} = 1\,\mathrm{mm}$. The cross-sectional area, the elastic section modulus, and the moment of inertia are given by

$$\bar{A} = \bar{t}\bar{w} = 1\,\mathrm{mm}^2, \quad \bar{Z} = \frac{1}{6}\bar{t}\bar{w}^2 = \frac{1}{6}\,\mathrm{mm}^3, \quad \bar{I} = \frac{1}{12}\bar{t}\bar{w}^3 = \frac{1}{12}\,\mathrm{mm}^4.$$

The shear correction factor of Timoshenko elements is $\kappa = 5/6$.

The material parameters of two constituent materials, approximating an aluminium alloy (7075-T6) and a titanium alloy (Ti-6Al-4V), are listed in Table 2. The temperature change is $\Delta T = 200\,\mathrm{K}$. The side length of a unit cell is $l_{\mathrm{cell}} = 24\,\mathrm{mm}$. Concerning the compliance constraint in (30h), the upper bound for the compliance is $c^{\mathrm{u}} = 10^{-2}\,\mathrm{J}$ $(= 10^{-2}\,\mathrm{N}\cdot\mathrm{m})$ and a force of $1\,\mathrm{N}$ is applied as fictitious external load $\tilde{\boldsymbol{f}}$.

5.1 Example (I)

This section presents the results obtained by solving problem (30) in section 3.2. Hence, the separation constraint on material distributions is not considered. As for connection pattern of base cells, the two cases shown in Figure 1 are considered. We consider the two ground structures shown in Figure 7. The frame structure in Figure 7(a) consists of $|\mathcal{V}| = 3 \times 3 = 9$ nodes and $|\mathcal{E}| = 28$ members, while the one in Figure 7(b) consists of $|\mathcal{V}| = 4 \times 4 = 16$ nodes and $|\mathcal{E}| = 66$ members.

Table 2: Material properties of the constituent materials used in the numerical examples.

	Material 1 ($\mathcal{M}_1$)	Material 2 ($\mathcal{M}_2$)
Young's modulus	$\bar{E}_1 = 70\,\mathrm{GPa}$	$\bar{E}_2 = 110\,\mathrm{GPa}$
Shear modulus	$\bar{G}_1 = 25\,\mathrm{GPa}$	$\bar{G}_2 = 45\,\mathrm{GPa}$
Thermal expansion coefficient	$\bar{\alpha}_1 = 25 \times 10^{-6}\,\mathrm{K}^{-1}$	$\bar{\alpha}_2 = 10 \times 10^{-6}\,\mathrm{K}^{-1}$
Upper bound for stress	$\bar{\sigma}_1^{\mathrm{u}} = 340\,\mathrm{MPa}$	$\bar{\sigma}_2^{\mathrm{u}} = 860\,\mathrm{MPa}$

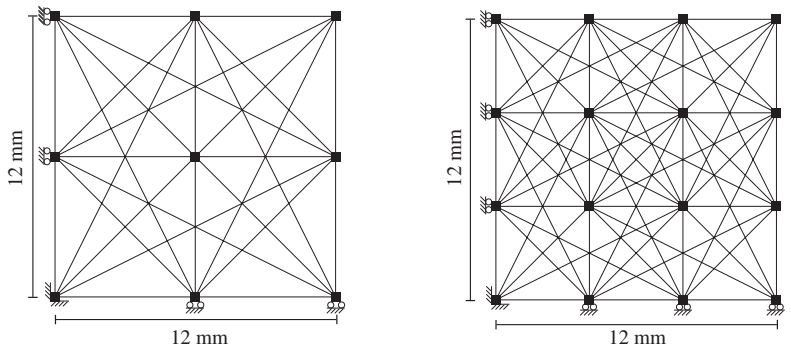

(a) (b)

Figure 7: The ground structures for example (I). (a) The frame structure with $|\mathcal{V}| = 3 \times 3$ nodes; and (b) the frame structure with $|\mathcal{V}| = 4 \times 4$ nodes.

5.1.1 Connection pattern (A) of example (I)

We begin with the results for connection pattern (A). The optimal solutions obtained for the two ground structures are shown in Figure 8(a) and Figure 8(c). In these figures, black lines and gray lines show members that consist of material 1 ($\mathcal{M}_1$) and material 2 ($\mathcal{M}_2$), respectively. The computational results are listed in Table 3. Here, "Time" shows the computational time spent by CPLEX [28], and the optimal value means the displacement of the interface node. Since the optimal values are negative in both cases, structures possessing thermal contraction properties are successfully obtained. CPLEX requires more than 66 hours to solve the optimization problem with the larger ground structure in Figure 7(b).

Figure 8(b) and Figure 8(d) show the optimized base cells. Deformations due to the thermal increase, $\Delta T = 200\,\mathrm{K}$, are also depicted in these figures, where displacements are magnified 20 times. It is observed in Figure 8(b) that $\mathcal{M}_1$, i.e., the material with the higher thermal expansion coefficient, forms star-shaped octagons, i.e., octagons with four reentrant corners. Also, in Figure 8(d) we can find a reentrant polygon consisting of $\mathcal{M}_1$. Similar shapes can be found in structures with negative Poisson's ratio [58]; see, e.g., [33, 34, 67] for star-shaped structures with negative Poisson's ratio.

5.1.2 Connection pattern (B) of example (I)

We next consider connection pattern (B). The two ground structures in Figure 7 are used. For connection pattern (B), we minimize the vertical displacement of the top-right node.

Table 3: Computational results of example (I).

$\lvert\mathcal{V}\rvert$	Pattern	Time (s)	Optimal value (mm)
3×3	(A)	14.22	-6.8785×10^{-2}
4×4	(A)	237712.69	-10.0626×10^{-2}
3×3	(B)	23.31	-0.8437×10^{-2}
4×4	(B)	490286.82	-4.6005×10^{-2}

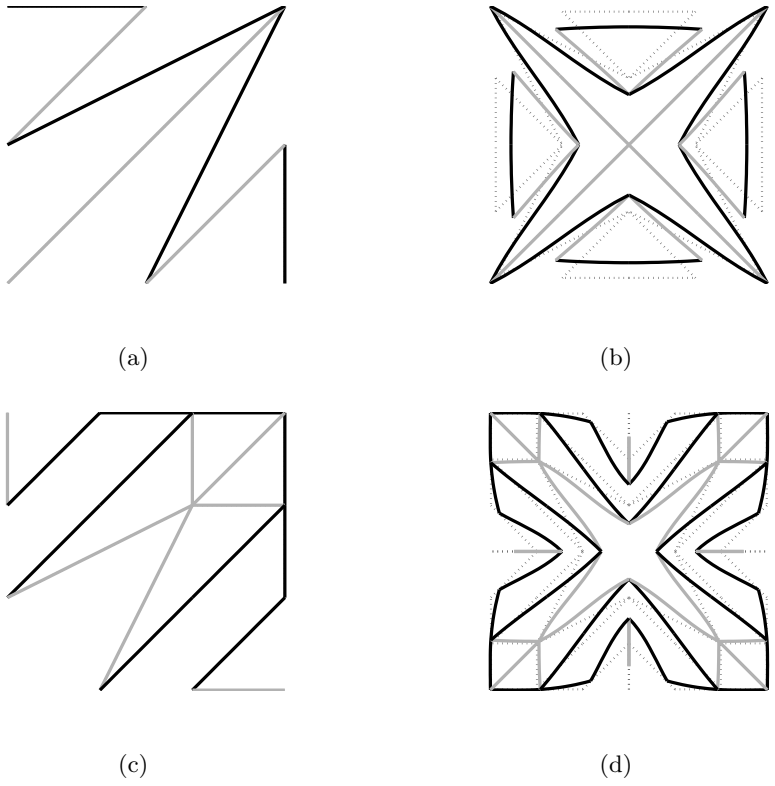

Figure 8: The optimal solutions of example (I) with connection pattern (A). (a) The optimal topology obtained from the ground structure in Figure 7(a); and (b) its deformed configuration at the high temperature. (c) The optimal topology obtained from the ground structure in Figure 7(b); and (d) its deformed configuration at the high temperature. Black lines show $\mathcal{M}_1$ (material 1) and gray lines show $\mathcal{M}_2$ (material 2). Displacements in (b) and (d) are magnified 20 times.

The optimal solutions are shown in Figure 9(a) and Figure 9(c). The computational results are listed in Table 3. Figure 9(b) and Figure 9(d) show the thermal deformations of the optimized base cells. Material 1 ($\mathcal{M}_1$) in Figure 9(b) forms a dodecagon with four reentrant corners. In Figure 9(d), we can find a star-shaped octagon consists of material 1. In this base cell, distributions of the two materials are intricately mixed. In contrast, distributions in Figure 9(b) are separated quite clearly. Indeed, in this solution, the four exterior members consisting of material 2 are used for connection with adjacent cells can be replaced by material 1, although this makes the objective value worse a little. The negative thermal expansion property stems mainly from the reentrant dodecagon and its interior members.

The optimized base cells obtained in section 5.1.1 and section 5.1.2 have the following characteristics; see Figures 8(b), 8(d), 9(b), and 9(d). The material with high thermal expansion ($\mathcal{M}_1$) forms a polygon with some reentrant corners. A structure consisting of the material with low thermal expansion ($\mathcal{M}_2$) is placed inside of the polygon. When temperature is elevated, expansion of the polygon is partially blocked by the interior structure and, as a result, the reentrant corners of the polygon move towards interior of the base cell. This explains the negative thermal expansion properties of the obtained solutions. Also, from this observation we see that the interfaces between the two different materials, i.e., the interfaces of the reentrant polygon ($\mathcal{M}_1$) and its interior structure

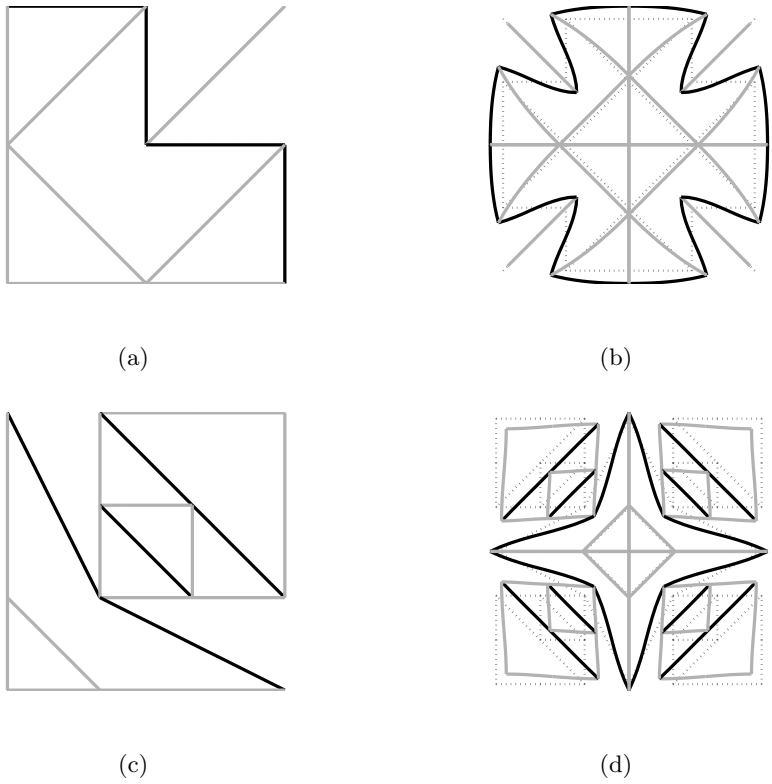

Figure 9: The optimal solutions of example (I) with connection pattern (B). (a) The optimal topology obtained from the ground structure in Figure 7(a); and (b) its deformed configuration at the high temperature (displacements are magnified 50 times). (c) The optimal topology obtained from the ground structure in Figure 7(b); and (d) its deformed configuration at the high temperature (displacements are magnified 20 times). Black lines show $\mathcal{M}_1$ (material 1) and gray lines show $\mathcal{M}_2$ (material 2).

($\mathcal{M}_2$), primarily undergo tension forces. In contrast, in section 5.2 we explore base cells such that $\mathcal{M}_1$ is surrounded by $\mathcal{M}_2$ by using the formulation developed in section 4. In such a solution we expect that the interfaces between the two different materials undergo compression forces.

5.2 Example (II)

This section performs the numerical experiments that incorporates the separation constraint on material distribution, which has been presented in section 4. We consider the two ground structures shown in Figure 10. The frame structure in Figure 10(a) consists of $|\mathcal{V}| = 3 \times 3$ nodes and $|\mathcal{E}| = 20$ members, while the one in Figure 10(b) consists of $|\mathcal{V}| = 4 \times 4$ nodes and $|\mathcal{E}| = 42$ members. As for connection pattern of base cells, the two cases shown in Figure 1 are considered.

5.2.1 Connection pattern (A) of example (II)

We first consider connection pattern (A). The optimal solutions obtained for the two ground structures in Figure 10 are shown in Figure 11(a) and Figure 11(c). Figure 11(b) and Figure 11(d) show the thermal deformations of the optimal base cells. It is observed in these figures that $\mathcal{M}_2$,

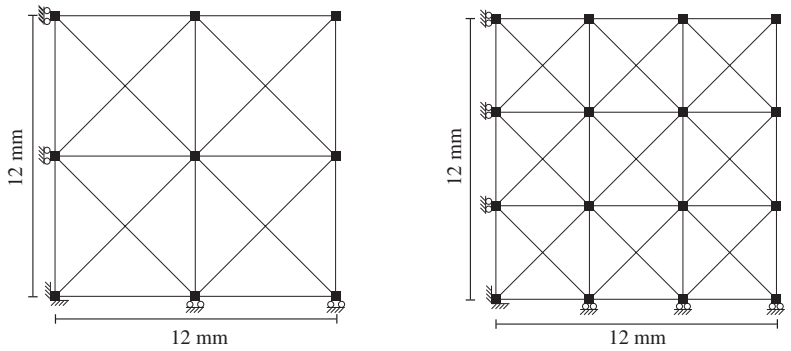

(a) (b)

Figure 10: The ground structures for example (II). (a) The frame structure with $|\mathcal{V}| = 3 \times 3$ nodes; and (b) the frame structure with $|\mathcal{V}| = 4 \times 4$nodes.

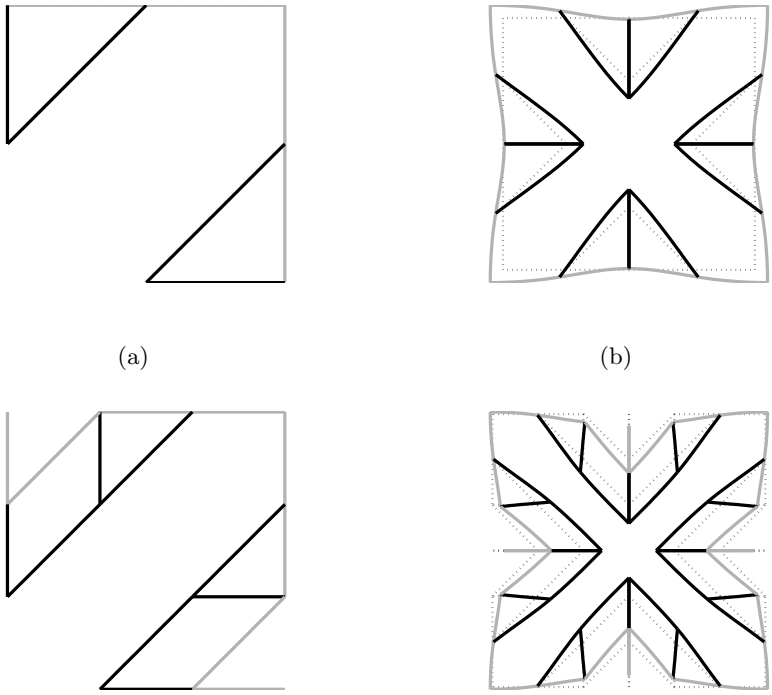

(a) (b)

(c) (d)

Figure 11: The optimal solutions of example (II) with connection pattern (A). (a) The optimal topology obtained from the ground structure in Figure 10(a); and (b) its deformed configuration at the high temperature (displacements are magnified 50 times). (c) The optimal topology obtained from the ground structure in Figure 10(b); and (d) its deformed configuration at the high temperature (displacements are magnified 20 times). Black lines show $\mathcal{M}_1$ (material 1) and gray lines show $\mathcal{M}_2$ (material 2).

i.e., the material with lower thermal expansion coefficient, is distributed on the outer side of $\mathcal{M}_1$, i.e., the one with the higher thermal expansion coefficient. Moreover, in Figure 11(d), $\mathcal{M}_1$ forms a hexadecagon with four reentrant corners.

The computational time and the optimal values are listed in Table 4. It is observed that in both cases the optimal solutions realize thermal contraction. CPLEX requires about 2.6 hours to solve the larger problem.

5.2.2 Connection pattern (B) of example (II)

We next consider connection pattern (B) in example (II). The obtained optimal solutions are shown in Figure 12(a) and Figure 12(c). The thermal deformations of the optimal base cells are depicted in Figure 12(b) and Figure 12(d). The computational costs and the optimal values are listed in Table 4. In this examples, both solutions do not exhibit negative thermal expansion.

Finally we discuss properties of the optimal solutions obtained in section 5.2.1 and section 5.2.2; see Figures 11(b), 11(d), 12(b), and 12(d). The low thermal expansion material ($\mathcal{M}_2$) is placed outside of the high thermal expansion material ($\mathcal{M}_1$), as expected. Particularly, it is observed in Figure 12(d) that, when temperature is elevated, the four interfaces between $\mathcal{M}_1$ and $\mathcal{M}_2$ undergo compression forces. Therefore, bonding between two materials is automatically strengthened by elevation of temperature. From a practical point of view, this might be an advantage over the solutions obtained in section 5.1. However, the solution in Figure 12(d) has a, very small but, nonnegative thermal expansion coefficient. Essential mechanism from which near zero thermal expansion stems is similar to the ones studied by Steeves *et al.* [60]. In the solutions shown in Figures 11(b), 11(d), and 12(b), the interior structures consisting of material 1 ($\mathcal{M}_1$) are disconnected. Further study is required to obtain a base cell with negative thermal expansion property and a connected interior structure consisting of $\mathcal{M}_1$.

6 Conclusions

Materials and structures that exhibit negative thermal expansion have been received significant interest because of their potential applications. This paper has addressed an optimization problem of a planar periodic frame structure, where the displacement induced by temperature increase is minimized. Numerical experiments showed that periodic frame structures demonstrating thermal contraction can be designed by using two materials with positive thermal expansion coefficients.

The problem dealt with in this paper is considered a three-phase material distribution problem

Table 4: Computational results of example (II).

$\lvert\mathcal{V}\rvert$	Pattern	Time (s)	Optimal value (mm)
3×3	(A)	7.02	-0.2597×10^{-2}
4×4	(A)	9499.49	-5.1059×10^{-2}
3×3	(B)	5.77	2.3919×10^{-2}
4×4	(B)	11269.00	0.1864×10^{-2}

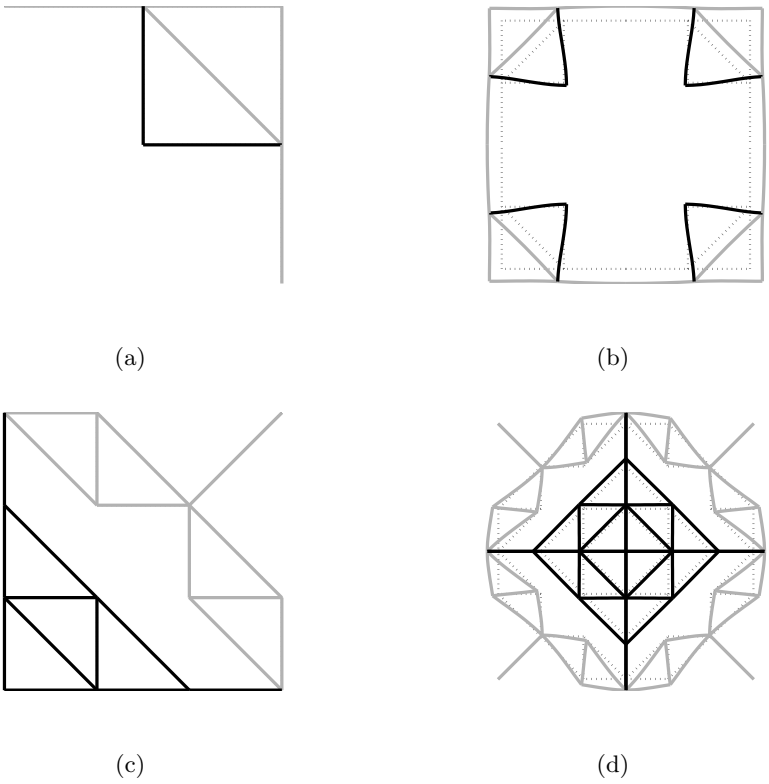

Figure 12: The optimal solutions of example (II) with connection pattern (B). (a) The optimal topology obtained from the ground structure in Figure 10(a); and (b) its deformed configuration at the high temperature (displacements are magnified 50 times). (c) The optimal topology obtained from the ground structure in Figure 10(b); and (d) its deformed configuration at the high temperature (displacements are magnified 20 times). Black lines show $\mathcal{M}_1$ (material 1) and gray lines show $\mathcal{M}_2$ (material 2).

for a given frame structure. Namely, we solve an optimization problem to select the material for each member among from two specified materials and void. In the course of optimization, this material selection is handled by making use of two binary design variables. Also, local stress constraints are fully addressed and existing members have predetermined sections. As a result, the optimal structure obtained by the proposed method has neither hinges nor thin members. In this respect the proposed approach may have an advantage in ease of manufacture of the optimal solution. It is worth noting that solutions with hinge-like regions and/or too thin members often require that, in advance of manufacturing process, thickness of hinges should be adjusted carefully to avoid stress concentration without losing thermal contraction properties.

In this paper the optimization problem has been recast as a mixed-integer linear programming (MILP) problem and solved globally with a commercial software package for MILP. It seems to be difficult to solve large-scale problems by this approach from a viewpoint of computational cost. Some heuristic methods, which can find a local optimal solution of a large-scale problem within reasonable computational time, remain to be explored. Particularly, the local search with MILP, that was initiated for topology optimization by Stolpe and Stidsen [65] and applied to frame structures by Kureta and Kanno [33], could be applied. In this paper we restrict ourselves to finding a structure

with the minimum thermal expansion coefficient, where the displacement of the interface node for cell connection, u_1, is minimized. The presented formulation can be extended straightforwardly to a problem finding a structure with a nearly zero thermal expansion coefficient. Namely, we can replace the objective function, u_1, by $|u_1|$. The optimization problem can still be recast as an MILP problem.

In the optimal solution distributions of the two materials can be complicated. With an intricate mixture pattern, a large number of interfaces between two different materials exist in a base cell and many small parts may be required in real manufacturing process. This may cause difficulty in fabrication of a base cell. Section 4 has explored a formulation for avoiding mixture of materials. In this formulation, binary variables are allocated to nodes to determine a material that can be used for each member. Then we consider linear inequality constraints to guarantee that one material is placed only outside of the other one. This formulation, however, limits the solution space excessively. In other words, the formulation excludes several designs with two disjoint material distributions. Also, explicit forms of the linear inequality constraints depend on topology of a ground structure. Hence, for the separation constraints on material distributions, more sophisticated formulations that can express any acceptable solutions remain to be explored.

Concerning negative thermal expansion coefficient behavior, this paper has addressed minimization of the displacement of a node that serves as an interface for periodic connection of base unit cells. Two connection patterns have been considered, where the shape of base cell is supposed to be square. Other shapes of base cell, as well as other connection patterns, remain to be studied. It might be preferable that the connection pattern and the base cell topology are optimized simultaneously. From a practical point of view, issues of geometrical nonlinearity and out-of-plane deformations may possibly have to be considered. Extensions to three-dimensional structures also remain to be explored.

Acknowledgments

The work of the second author is partially supported by Grant-in-Aid for Scientific Research (C) 23560663 and by the Aihara Project, the FIRST program from JSPS, initiated by CSTP.

References

[1] Achterberg, T.: SCIP: Solving constraint integer programs. *Mathematical Programming Computation*, **1**, 1–41 (2009).

[2] Achtziger, W., Kanzow, C.: Mathematical programs with vanishing constraints: Optimality conditions and constraint qualifications. *Mathematical Programming*, **A114**, 69–99 (2008).

[3] Allaire, G., Jouve, F.: Minimum stress optimal design with the level set method. *Engineering Analysis with Boundary Elements*, **32**, 909–918 (2008).

[4] Barrera, G.D., Bruno, J.A.O., Barron, T.H.K., Allan, N.L.: Negative thermal expansion. *Journal of Physics: Condensed Matter*, **17**, R217–R252 (2005).

[5] Baughman, R.H., Galvão, D.S.: Crystalline networks with unusual predicted mechanical and thermal properties. *Nature*, **365**, 735–737 (1993).

[6] Bruggi, M.: On an alternative approach to stress constraints relaxation in topology optimization. *Structural and Multidisciplinary Optimization*, **36**, 125–141 (2008).

[7] Bruyneel, M.: SFP—A new parameterization based on shape functions for optimal material selection: Application to conventional composite plies. *Structural and Multidisciplinary Optimization*, **43**, 17–27 (2011).

[8] Chen, B.-C., Kikuchi, N.: Topology optimization with design-dependent loads. *Finite Elements in Analysis and Design*, **37**, 57–70 (2001).

[9] Chen, B.-C., Silva, E.C.N., Kikuchi, N.: Advances in computational design and optimization with application to MEMS. *International Journal for Numerical Methods in Engineering*, **52**, 23–62 (2001).

[10] Cheng, G.D., Guo, X.: ε-relaxed approach in structural topology optimization. *Structural Optimization*, **13**, 258–266 (1997).

[11] Deaton, J.D., Grandhi, R.V.: Stiffening of restrained thermal structures via topology optimization. *Structural and Multidisciplinary Optimization*, **48**, 731–745 (2013).

[12] Deng, J., Yan, J., Cheng, G.: Multi-objective concurrent topology optimization of thermoelastic structures composed of homogeneous porous material. *Structural and Multidisciplinary Optimization*, **47**, 583–597 (2013).

[13] Duysinx, P., Bendsøe, M.P.: Topology optimization of continuum structures with local stress constraints. *International Journal for Numerical Methods in Engineering*, **43**, 1453–1478 (1998).

[14] Evans, J.S.O.: Negative thermal expansion materials. *Journal of the Chemical Society, Dalton Transactions*, 33317–3326 (1999).

[15] Evans, J.S.O., David, W.I.F., Sleight, A.W.: Structural investigation of the negative-thermal-expansion material ZrW_2O_8. *Acta Crystallographica*, **B55**, 333–340 (1999).

[16] Friedman, Z., Kosmatka, B.: An improved two-node Timoshenko beam finite element. *Computers and Structures*, **47**, 473–481 (1993).

[17] Gao, T., Zhang, W.: Topology optimization involving thermo-elastic stress loads. *Structural and Multidisciplinary Optimization*, **42**, 725–738 (2010).

[18] Gibiansky, L.V., Sigmund, O.: Multiphase composites with extremal bulk modulus. *Journal of the Mechanics and Physics of Solids*, **48**, 461–498 (2000).

[19] Gibiansky, L.V., Torquato, S.: Thermal expansion of isotropic multiphase composites and polycrystals. *Journal of the Mechanics and Physics of Solids*, **45**, 1223–1252 (1997).

[20] Grima, J.N., Ellul, B., Attard, D., Gatt, R., Attard, M.: Composites with needle-like inclusions exhibiting negative thermal expansion: A preliminary investigation. *Composites Science and Technology*, **70**, 2248–2252 (2010).

[21] Grima, J.N., Ellul, B., Gatt, R., Attard, D.: Negative thermal expansion from disc, cylindrical, and needle shaped inclusions. *Physica Status Solidi (B)*, **250**, 2051–2056 (2013).

[22] Grima, J.N., Farrugia, P.S., Gatt, R., Zammit, V.: A system with adjustable positive or negative thermal expansion. *Proceedings of the Royal Society, A*, **463**, 1585–1596 (2007).

[23] Grima, J.N., Oliveri, L., Ellul, B., Gatt, R., Attard, D., Cicala, G., Recca, G.: Adjustable and negative thermal expansion from multilayered systems. *Physica Status Solidi (Rapid Research Letters)*, **4**, 133–135 (2010).

[24] Guo, X., Zhang, W.S., Wang, M.Y., Wei, P.: Stress-related topology optimization via level set approach. *Computer Methods in Applied Mechanics and Engineering*, **200**, 3439–3452 (2011).

[25] Gurobi Optimization, Inc.: *Gurobi Optimizer Reference Manual*. `http://www.gurobi.com/` (Accessed October 2013).

[26] Holmberg, E., Torstenfelt, B., Klarbring, A.: Stress constrained topology optimization. *Structural and Multidisciplinary Optimization*, **48**, 33–47 (2013).

[27] Hvejsel, C.F., Lund, E.: Material interpolation schemes for unified topology and multi-material optimization. *Structural and Multidisciplinary Optimization*, **43**, 811–825 (2011).

[28] IBM ILOG: *User's Manual for CPLEX*. `http://www.ilog.com/` (Accessed October 2013).

[29] Jacquot, P., Lehmann, M., Colonna de Lega, X.: Deformation analysis of a communication telescope structure under non-uniform heating using holographic interferometry. *Proceedings of the International Society for Optical Engineering*, **3293**, 102–113 (1998).

[30] Jefferson, G., Parthasarathy, T.A., Kerans, R.J.: Tailorable thermal expansion hybrid structures. *International Journal of Solids and Structures*, **46**, 2372–2387 (2009).

[31] Jog, C.: Distributed-parameter optimization and topology design for non-linear thermoelasticity. *Computer Methods in Applied Mechanics and Engineering*, **132**, 117–134 (1996).

[32] Kanno, Y.: Topology optimization of tensegrity structures under compliance constraint: A mixed integer linear programming approach. *Optimization and Engineering*, **14**, 61–96 (2013).

[33] Kureta, R., Kanno, Y.: A mixed integer programming approach to designing periodic frame structures with negative Poisson's ratio. *Optimization and Engineering*, to appear.

[34] Lakes, R.: Foam structures with a negative Poisson's ratio. *Science*, **235**, 1038–1040 (1987).

[35] Lakes, R.: Cellular solid structures with unbounded thermal expansion. *Journal of Materials Science Letters*, **15**, 475–477 (1996).

[36] Li, Y., Saitou, K., Kikuchi, N.: Topology optimization of thermally actuated compliant mechanisms considering time-transient effect. *Finite Elements in Analysis and Design*, **40**, 1317–1331 (2004).

[37] Lightfoot, P., Woodcock, D.A., Maple, M.J., Villaescusa, L.A., Wright, P.A.: The widespread occurrence of negative thermal expansion in zeolites. *Journal of Materials Chemistry*, **11**, 212–216 (2001).

[38] Lim, T.: Anisotropic and negative thermal expansion behavior in a cellular microstructure. *Journal of Materials Science*, **40**, 3275–3277 (2005).

[39] Lim, T.: Negative thermal expansion structures constructed from positive thermal expansion trusses. *Journal of Materials Science*, **47**, 368–373 (2012).

[40] Lind, C.: Two decades of negative thermal expansion research: Where do we stand? *Materials*, **5**, 1125–1154 (2012).

[41] MacNeal, R.H.: A simple quadrilateral shell element. *Computers and Structures*, **8**, 175–183 (1978).

[42] Martinek, C., Hummel, F.A.: Linear thermal expansion of three tungstates. *Journal of the American Ceramic Society*, **51**, 227–228 (1968).

[43] Miller, W., Mackenzie, D.S., Smith, C.W., Evans, K.E.: A generalised scale-independent mechanism for tailoring of thermal expansivity: Positive and negative. *Mechanics of Materials*, **40**, 351–361 (2008).

[44] Miller, W., Smith, C.W., Mackenzie, D.S., Evans, K.E.: Negative thermal expansion: A review. *Journal of Materials Science*, **44**, 5441–5451 (2009).

[45] Palumbo, N.M.A., Smith, C.W., Miller, W., Evans, K.E.: Near-zero thermal expansivity 2-D lattice structures: Performance in terms of mass and mechanical properties. *Acta Materialia*, **59**, 2392–2403 (2011).

[46] Pedersen, P., Pedersen, N.L.: Strength optimized designs of thermoelastic structures. *Structural and Multidisciplinary Optimization*, **42**, 681–691 (2010).

[47] Pedersen, P., Pedersen, N.L.: Interpolation/penalization applied for strength design of 3D thermoelastic structures. *Structural and Multidisciplinary Optimization*, **45**, 773–786 (2012).

[48] Poulsen, T.A.: A new scheme for imposing a minimum length scale in topology optimization. *International Journal for Numerical Methods in Engineering*, **57**, 741–760 (2003).

[49] Qi, J., Halloran, J.W.: Negative thermal expansion artificial material from iron-nickel alloys by oxide co-extrusion with reductive sintering. *Journal of Materials Science*, **39**, 4113–4118 (2004).

[50] Ramirez, A.P., Kowach, G.R.: Large low temperature specific heat in the negative thermal expansion compound ZrW_2O_8. *Physical Review Letters*, **80**, 4903–4906 (1998).

[51] Rasmussen, M.H., Stolpe, M.: Global optimization of discrete truss topology design problems using a parallel cut-and-branch method. *Computers and Structures*, **86**, 1527–1538 (2008).

[52] Reddy, J.N.: On locking-free shear deformable beam finite elements. *Computer Methods in Applied Mechanics and Engineering*, **149**, 113–132 (1997).

[53] Rodrigues, H., Fernandes, P.: A material based model for topology optimization of thermoelastic structures. *International Journal for Numerical Methods in Engineering*, **38**, 1951–1965 (1995).

[54] Rozvany, G.I.N.: On design-dependent constraints and singular topologies. *Structural and Multidisciplinary Optimization*, **21**, 164–172 (2001).

[55] Sigmund, O.: Design of multiphysics actuators using topology optimization—Part II: Two-material structures. *Computer Methods in Applied Mechanics and Engineering*, **190**, 6605–6627 (2001).

[56] Sigmund, O.: Morphology-based black and white filters for topology optimization. *Structural and Multidisciplinary Optimization*, **33**, 401–424 (2007).

[57] Sigmund, O., Torquato, S.: Composites with extremal thermal expansion coefficients. *Applied Physics Letters*, **69**, 3203–3205 (1996).

[58] Sigmund, O., Torquato, S.: Design of materials with extreme thermal expansion using a three-phase topology optimization method. *Journal of the Mechanics and Physics of Solids*, **45**, 1037–1067 (1997).

[59] Sleight, A.W.: Isotropic negative thermal expansion. *Annual Review of Materials Science*, **28**, 29–43 (1998).

[60] Steeves, C.A., dos Santos e Lucato, S.L., He, M., Antinucci, E., Hutchinson, J.W., Evans, A.G.: Concepts for structurally robust materials that combine low thermal expansion with high stiffness. *Journal of the Mechanics and Physics of Solids*, **55**, 1803–1822 (2007).

[61] Steeves, C.A., Evans, A.G.: Optimization of thermal protection systems utilizing sandwich structures with low coefficient of thermal expansion lattice hot faces. *Journal of the American Ceramic Society*, **94**, S55–S61 (2011).

[62] Steeves, C.A., Mercer, C., Antinucci, E., He, M.Y., Evans, A.G.: Experimental investigation of the thermal properties of tailored expansion lattices. *International Journal of Mechanics and Materials in Design*, **5**, 195–202 (2009).

[63] Stegmann, J., Lund, E.: Discrete material optimization of general composite shell structures. *International Journal for Numerical Methods in Engineering*, **62**, 2009–2027 (2005).

[64] Stolpe, M.: On the reformulation of topology optimization problems as linear or convex quadratic mixed 0–1 programs. *Optimization and Engineering*, **8**, 163–192 (2007).

[65] Stolpe, M., Stidsen, T.: A hierarchical method for discrete structural topology design problems with local stress and displacement constraints. *International Journal for Numerical Methods in Engineering*, **69**, 1060–1084 (2007).

[66] Stolpe, M., Svanberg, K.: Modelling topology optimization problems as linear mixed 0–1 programs. *International Journal for Numerical Methods in Engineering*, **57**, 723–739 (2003).

[67] Theocaris, P.S., Stavroulakis, G.E., Panagiotopoulos, P.D.: Negative Poisson's ratios in composites with star-shaped inclusions: A numerical homogenization approach. *Archive of Applied Mechanics*, **67**, 274–286 (1997).

[68] Tortorelli, D.A., Subramani, G., Lu, S.C.Y., Haber, R.B.: Sensitivity analysis for coupled thermoelastic systems. *International Journal of Solids and Structures*, **27**, 1477–1497 (1991).

[69] Wang, M.Y., Wang, X.: "Color" level sets: A multi-phase method for structural topology optimization with multiple materials. *Computer Methods in Applied Mechanics and Engineering*, **193**, 469–496 (2004).

[70] Wang, B., Yan, J., Cheng, G.: Optimal structure design with low thermal directional expansion and high stiffness. *Engineering Optimization*, **43**, 581–595, (2011).

[71] Xia, Q., Wang, M.Y.: Topology optimization of thermoelastic structures using level set method. *Computational Mechanics*, **42**, 837–857 (2008).

[72] Yoon, G.H., Kim, Y.Y., Bendsøe, M.P., Sigmund, O.: Hinge-free topology optimization with embedded translation-invariant differentiable wavelet shrinkage. *Structural and Multidisciplinary Optimization*, **27**, 139–150 (2004).

[73] Zhou, S., Wang, M.Y.: Multimaterial structural topology optimization with a generalized Cahn–Hilliard model of multiphase transition. *Structural and Multidisciplinary Optimization*, **33**, 89–111 (2007).

[74] Zhu, B., Zhang, X., Wang, N.: Topology optimization of hinge-free compliant mechanisms with multiple outputs using level set method. *Structural and Multidisciplinary Optimization*, **47**, 659–672 (2013).

A Decomposition of equilibrium equations

According to [33], we decompose the stiffness matrix, $K(\boldsymbol{E}, \boldsymbol{G})$, in (9b) and (9d). The results obtained below have been used in section 3.1; see (15) and (16).

Consider the local coordinate system for member $e = (i, j) \in \mathcal{E}$ as shown in Figure 13. The element displacement vector is written as $\hat{\boldsymbol{u}}_e = (u_x^{(i)}, u_y^{(i)}, \theta^{(i)}, u_x^{(j)}, u_y^{(j)}, \theta^{(j)})^\top \in \mathbb{R}^6$. The displacement vector of the whole ground structure, $\boldsymbol{u} \in \mathbb{R}^d$, is defined with respect to the global coordinate system. For each $e \in \mathcal{E}$, transformation of $\boldsymbol{u}$ to $\hat{\boldsymbol{u}}_e$ is written as

$$\hat{\boldsymbol{u}}_e = T_e \boldsymbol{u},$$

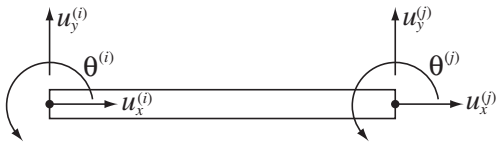

Figure 13: Local coordinate system for a beam element.

where $T_e \in \mathbb{R}^{6\times d}$ is a constant transformation matrix. We employ the Timoshenko beam theory to model the members of the ground structure. Let $\hat{K}_e(E_e, G_e) \in \mathbb{R}^{6\times 6}$ denote the member stiffness matrix defined with respect to the local coordinate system. As explained in [33], $\hat{K}_e$ is given by

$$\hat{K}_e(E_e, G_e) = \sum_{t=1}^{3} k_{et}(E_e, G_e)\hat{\boldsymbol{b}}_{et}\hat{\boldsymbol{b}}_{et}^{\top}, \tag{42}$$

where $\hat{\boldsymbol{b}}_{e1}$, $\hat{\boldsymbol{b}}_{e2}$, $\hat{\boldsymbol{b}}_{e3} \in \mathbb{R}^3$ are defined by

$$\hat{\boldsymbol{b}}_{e1} = \begin{bmatrix} -1 \\ 0 \\ 0 \\ 1 \\ 0 \\ 0 \end{bmatrix}, \quad \hat{\boldsymbol{b}}_{e2} = \begin{bmatrix} 0 \\ -1 \\ -l_e/2 \\ 0 \\ 1 \\ -l_e/2 \end{bmatrix}, \quad \hat{\boldsymbol{b}}_{e3} = \begin{bmatrix} 0 \\ 0 \\ -1 \\ 0 \\ 0 \\ 1 \end{bmatrix} \tag{43}$$

and k_{e1}, k_{e2}, $k_{e3} \in \mathbb{R}$ are defined by

$$k_{e1} = \frac{E_e A_e}{l_e}, \tag{44a}$$

$$k_{e2} = \frac{1}{l_e}\Big(\frac{l_e^2}{12E_eI_e} + \frac{1}{\kappa G_e A_e}\Big)^{-1}, \tag{44b}$$

$$k_{e3} = \frac{E_e I_e}{l_e}. \tag{44c}$$

Here, E_e and G_e are Young's modulus and the shear modulus of the beam material, A_e and I_e are the cross-sectional area and the moment of inertia, l_e is length of the beam element, and κ is the shear correction factor in the Timoshenko beam theory. In (44b), we define $k_{e2} = 0$ if $E_e = G_e = 0$ for convention. Note that (43) and (44) correspond to the MacNeal element in the Timoshenko beam theory [41]. In our problem, beams are subjected to nodal loads only. In this case, the MacNeal element coincides with the interdependent interpolation element in [52], and hence the nodal displacement of a beam can be predicted exactly with single element [16, 52].

For member $e = (i, j) \in \mathcal{E}$, let $\boldsymbol{s}_e = (s_{e1}, s_{e2}, s_{e3})^{\top} \in \mathbb{R}^3$ denote the generalized stress vector, which is defined by

$$s_{e1} = q_e, \tag{45a}$$

$$s_{e2} = \tau_e = -\frac{m_e^{(i)} + m_e^{(j)}}{l_e}, \tag{45b}$$

$$s_{e3} = \frac{-m_e^{(i)} + m_e^{(j)}}{2}. \tag{45c}$$

Here, q_e is the axial force, τ_e is the transverse shear force, and $m_e^{(i)}$ and $m_e^{(j)}$ are the two end moments. The force-balance equation in the global coordinate system is then given by

$$\sum_{e\in\mathcal{E}}\sum_{t=1}^{3} s_{et}\boldsymbol{b}_{et} = \boldsymbol{f}, \tag{46}$$

where constant vectors $\boldsymbol{b}_{e1}$, $\boldsymbol{b}_{e2}$, $\boldsymbol{b}_{e3} \in \mathbb{R}^d$ are defined by

$$\boldsymbol{b}_{et} = T_e^\top \hat{\boldsymbol{b}}_{et}, \quad t = 1, 2, 3. \tag{47}$$

The generalized stress, s_{et}, is related to the displacement, $\boldsymbol{u}$, as

$$s_{et} = k_{et}\boldsymbol{b}_{et}^\top \boldsymbol{u}, \quad t = 1, 2, 3;\ \forall e \in \mathcal{E}, \tag{48}$$

Since the global stiffness matrix, $K(\boldsymbol{E}, \boldsymbol{G})$, is given by

$$K(\boldsymbol{E}, \boldsymbol{G}) = \sum_{e\in\mathcal{E}} T_e^\top \hat{K}(E_e, G_e) T_e,$$

we can see that elimination of s_{et}'s from (46) and (48) results in the global equilibrium equation

$$K(\boldsymbol{E}, \boldsymbol{G})\boldsymbol{u} = \boldsymbol{f}.$$

Expression in (46) and (48) has served as basis of our MILP formulation.

B Whole perspective of MILP problem with domain separation constraint

In section 4, we have explained that the design optimization problem with the separation constraint on material domains can be recast as an MILP problem. The explicit description of this MILP problem is shown below.

We elaborate the MILP formulation in section 4.2 with comparing with MILP problem (30) in section 3.2, i.e., the one without the separation constraint. Firstly, the objective function is same as the one of problem (30). Namely, we minimize the displacement of the interface node, u_1.

Secondly, the constraints are given as follows.

- Constraints (30b), (30f), and (30h) are retained without change, i.e.,

$$\sum_{e\in\mathcal{E}}\sum_{t=1}^{3} s_{et}\boldsymbol{b}_{et} = \boldsymbol{f}, \tag{49}$$

$$\sum_{e\in\mathcal{E}}\sum_{t=1}^{3} \tilde{s}_{et}\boldsymbol{b}_{et} = \tilde{\boldsymbol{f}}, \tag{50}$$

$$\tilde{\boldsymbol{f}}^\top \tilde{\boldsymbol{u}} \le c^{\mathrm{u}}. \tag{51}$$

- Corresponding to constraints (30c) and (30d), relations between the generalized stresses and the displacements caused by the elevation of temperature are given as

$$\begin{aligned}
|s_{e1} - \bar{k}_{e11}(\boldsymbol{b}_{e1}^\top \boldsymbol{u} - l_e \bar{\alpha}_1 \Delta T)| &\le L(1 - x_e + z_i), && \forall e = (i,j),\\
|s_{e1} - \bar{k}_{e11}(\boldsymbol{b}_{e1}^\top \boldsymbol{u} - l_e \bar{\alpha}_1 \Delta T)| &\le L(1 - x_e + z_j), && \forall e = (i,j),\\
|s_{e1} - \bar{k}_{e12}(\boldsymbol{b}_{e1}^\top \boldsymbol{u} - l_e \bar{\alpha}_2 \Delta T)| &\le L(3 - x_e - z_i - z_j), && \forall e = (i,j),\\
|s_{e1}| &\le L x_e, && \forall e
\end{aligned}$$

and

$$\begin{aligned}
|s_{et} - \bar{k}_{et1}\boldsymbol{b}_{et}^\top \boldsymbol{u}| &\le L(1 - x_e + z_i), && t = 2,3;\ \forall e = (i,j),\\
|s_{et} - \bar{k}_{et1}\boldsymbol{b}_{et}^\top \boldsymbol{u}| &\le L(1 - x_e + z_j), && t = 2,3;\ \forall e = (i,j),\\
|s_{et} - \bar{k}_{et2}\boldsymbol{b}_{et}^\top \boldsymbol{u}| &\le L(3 - x_e - z_i - z_j), && t = 2,3;\ \forall e = (i,j),\\
|s_{et}| &\le L x_e, && t = 2,3;\ \forall e.
\end{aligned}$$

- Instead of (30e), the stress constraints at the elevated temperature are written as

$$\begin{aligned}
\frac{|s_{e1}|}{\bar{A}} + \frac{l_e|s_{e2}|}{2\bar{Z}} + \frac{|s_{e3}|}{\bar{Z}} &\le \bar{\sigma}_1^{\mathrm{u}}(2 - z_i - z_j) + \bar{\sigma}_2^{\mathrm{u}} z_i, && \forall e = (i,j),\\
\frac{|s_{e1}|}{\bar{A}} + \frac{l_e|s_{e2}|}{2\bar{Z}} + \frac{|s_{e3}|}{\bar{Z}} &\le \bar{\sigma}_1^{\mathrm{u}}(2 - z_i - z_j) + \bar{\sigma}_2^{\mathrm{u}} z_j, && \forall e = (i,j),\\
\frac{|s_{e1}|}{\bar{A}} + \frac{l_e|s_{e2}|}{2\bar{Z}} + \frac{|s_{e3}|}{\bar{Z}} &\le \bar{\sigma}_1^{\mathrm{u}}(1 + z_i + z_j) + \bar{\sigma}_2^{\mathrm{u}}(z_i + z_j), && \forall e = (i,j).
\end{aligned}$$

- Corresponding to constraint (30g), relations between the generalized stresses and the displacements caused by the fictitious external load are given as

$$\begin{aligned}
|\tilde{s}_{et} - \bar{k}_{et1}\boldsymbol{b}_{et}^\top \tilde{\boldsymbol{u}}| &\le L(1 - x_e + z_i) && t = 1,2,3;\ \forall e = (i,j),\\
|\tilde{s}_{et} - \bar{k}_{et1}\boldsymbol{b}_{et}^\top \tilde{\boldsymbol{u}}| &\le L(1 - x_e + z_j) && t = 1,2,3;\ \forall e = (i,j),\\
|\tilde{s}_{et} - \bar{k}_{et2}\boldsymbol{b}_{et}^\top \tilde{\boldsymbol{u}}| &\le L(3 - x_e - z_i - z_j) && t = 1,2,3;\ \forall e = (i,j),\\
|\tilde{s}_{et}| &\le L x_e && t = 1,2,3;\ \forall e.
\end{aligned}$$

- Instead of constraint (30i), the stress constraints at the ordinary temperature are given as

$$\begin{aligned}
\frac{|\tilde{s}_{e1}|}{\bar{A}} + \frac{l_e|\tilde{s}_{e2}|}{2\bar{Z}} + \frac{|\tilde{s}_{e3}|}{\bar{Z}} &\le \bar{\sigma}_1^{\mathrm{u}}(2 - z_i - z_j) + \bar{\sigma}_2^{\mathrm{u}} z_i, && \forall e = (i,j),\\
\frac{|\tilde{s}_{e1}|}{\bar{A}} + \frac{l_e|\tilde{s}_{e2}|}{2\bar{Z}} + \frac{|\tilde{s}_{e3}|}{\bar{Z}} &\le \bar{\sigma}_1^{\mathrm{u}}(2 - z_i - z_j) + \bar{\sigma}_2^{\mathrm{u}} z_j, && \forall e = (i,j),\\
\frac{|\tilde{s}_{e1}|}{\bar{A}} + \frac{l_e|\tilde{s}_{e2}|}{2\bar{Z}} + \frac{|\tilde{s}_{e3}|}{\bar{Z}} &\le \bar{\sigma}_1^{\mathrm{u}}(1 + z_i + z_j) + \bar{\sigma}_2^{\mathrm{u}}(z_i + z_j), && \forall e = (i,j).
\end{aligned}$$

- Instead of constraint (30j), the constraint prohibiting intersection of members is given as

$$x_e + x_{e'} \le 1, \quad \forall (e, e') \in \mathcal{E}_{\mathrm{cross}}.$$

- Concerning symmetry of the base cell, we have the following constraints:

$$\begin{aligned}
x_e &= x_{e'}, \quad \forall (e, e') \in \mathcal{E}_{\mathrm{sym}},\\
z_i &= z_j, \quad \forall (i,j) \in \mathcal{V}_{\mathrm{sym}}.
\end{aligned}$$

- Concerning separation of material distributions, we have the following constraints:

$$\begin{aligned} z_{r_1(i)} &\leq z_i, && \forall i \in \mathcal{V}_{\text{upper}}, \\ z_i &\leq z_{r_2(i)}, && \forall i \in \mathcal{V}_{\text{diag}}, \\ z_{r_1^{-1}(i)} &\leq z_i + z_{r_2(i)}, && \forall i \in \mathcal{V}_{\text{diag}}. \end{aligned}$$

- Finally, binary constraints are

$$\begin{aligned} x_e &\in \{0,1\}, && \forall e \in \mathcal{E}, \\ z_i &\in \{0,1\}, && \forall i \in \mathcal{V}. \end{aligned}$$

Thus the optimization problem is an MILP problem, where $\boldsymbol{u} \in \mathbb{R}^d$, $\tilde{\boldsymbol{u}} \in \mathbb{R}^d$, $s_{et} \in \mathbb{R}$, $\tilde{s}_{et} \in \mathbb{R}$, $x_e \in \{0,1\}$, and $s_i \in \{0,1\}$ ($\forall e \in \mathcal{E};\ \forall i \in \mathcal{V};\ t = 1,2,3$) are variables to be optimized.